Remote Sensing of Soils, Minerals, and Geomorphology

Carolina Distinguished Professor
Department of Geography
University of South Carolina
Columbia, South Carolina 29208
jrjensen@sc.edu

Remote Sensing of Soils, Minerals, and Geomorphology

- 26% of the Earth's surface is exposed land
- 74% of the Earth's surface is covered by water
- Almost all humanity lives on the terrestrial, solid Earth comprised of bedrock and the weathered bedrock called *soil*.
- Remote sensing can play a limited role in the identification, inventory, and mapping of *surficial soils* not covered with dense vegetation.
- Remote sensing can provide information about the *chemical composition* of rocks and minerals that are on the Earth's surface, and not completely covered by dense vegetation. Emphasis is placed on understanding unique *absorption bands* associated with specific types of rocks and minerals using imaging spectroscopy techniques.
- Remote sensing can also be used to extract *geologic information* including, lithology, structure, drainage patterns, and geomorphology (landforms).

Jensen, 2000

Soil Characteristics

• *Soil* is unconsolidated material at the surface of the Earth that serves as a natural medium for growing plants. Plant roots reside within this material and extract water and nutrients. Soil is the weathered material between the atmosphere at the Earth's surface and the bedrock below the surface to a maximum depth of approximately 200 cm (USDA, 1998).

• *Soil* is a mixture of inorganic mineral particles and organic matter of varying size and composition. The particles make up about 50 percent of the soil's volume. Pores containing air and/water occupy the remaining volume.

Jensen, 2000

Soil Taxonomy

• We no longer identify a "soil type". Rather, soil scientists determine the *soil taxonomy* (Petersen, 1999). *"Keys to Soil Taxonomy"* have been used by the USDA Natural Resources Conservation Service since 1975 to qualitatively and quantitatively differentiate between soil *taxa*. The highest category of the U.S. Soil Taxonomy is *Soil Order*. Each order reflects the dominant soil-forming processes and the degree of soil formation.

• There are 12 dominant U.S. *Soils Orders*: Alfisols (high-nutrient soils), Andisols (volcanic soils), Aridisols (desert soils), Entisols (new soils), Gelisols (tundra soils), Histosols (organic soils), Inceptisols (young soils), Mollisols (prairie soils), Oxisols (tropical soils),Spodosols (forest soils), Ultisols (low-nutrient sols), and Verticols (swelling-clay soils). Scientists use Dichotomous Keys to classify soils into Suborder, Great Groups, Subgroups, Family Level, and Soil Series.

Jensen, 2000

Standard Soil Profile (U.S. Department of Agriculture)

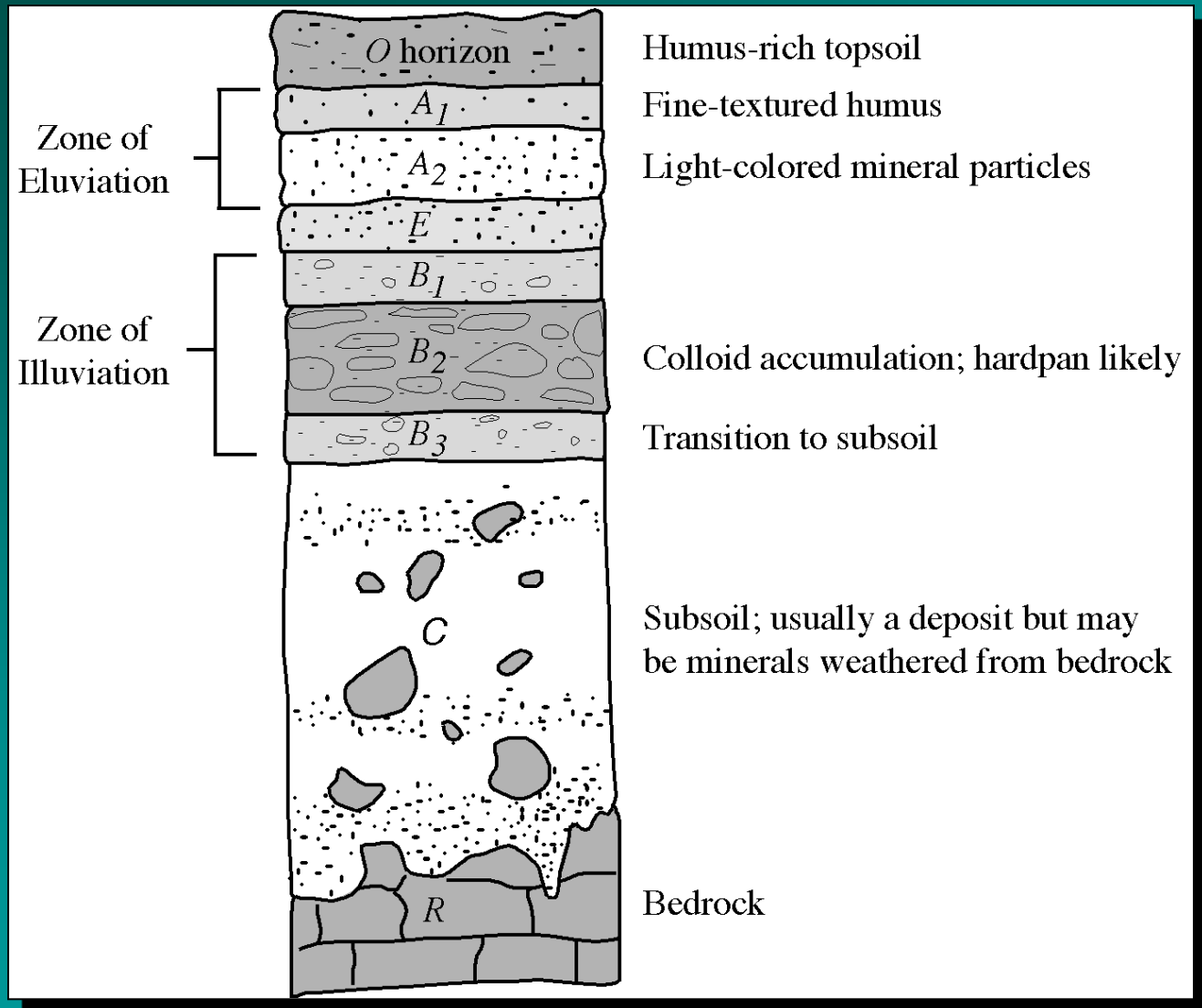

Jensen, 2000

Soil Particle Size Scales

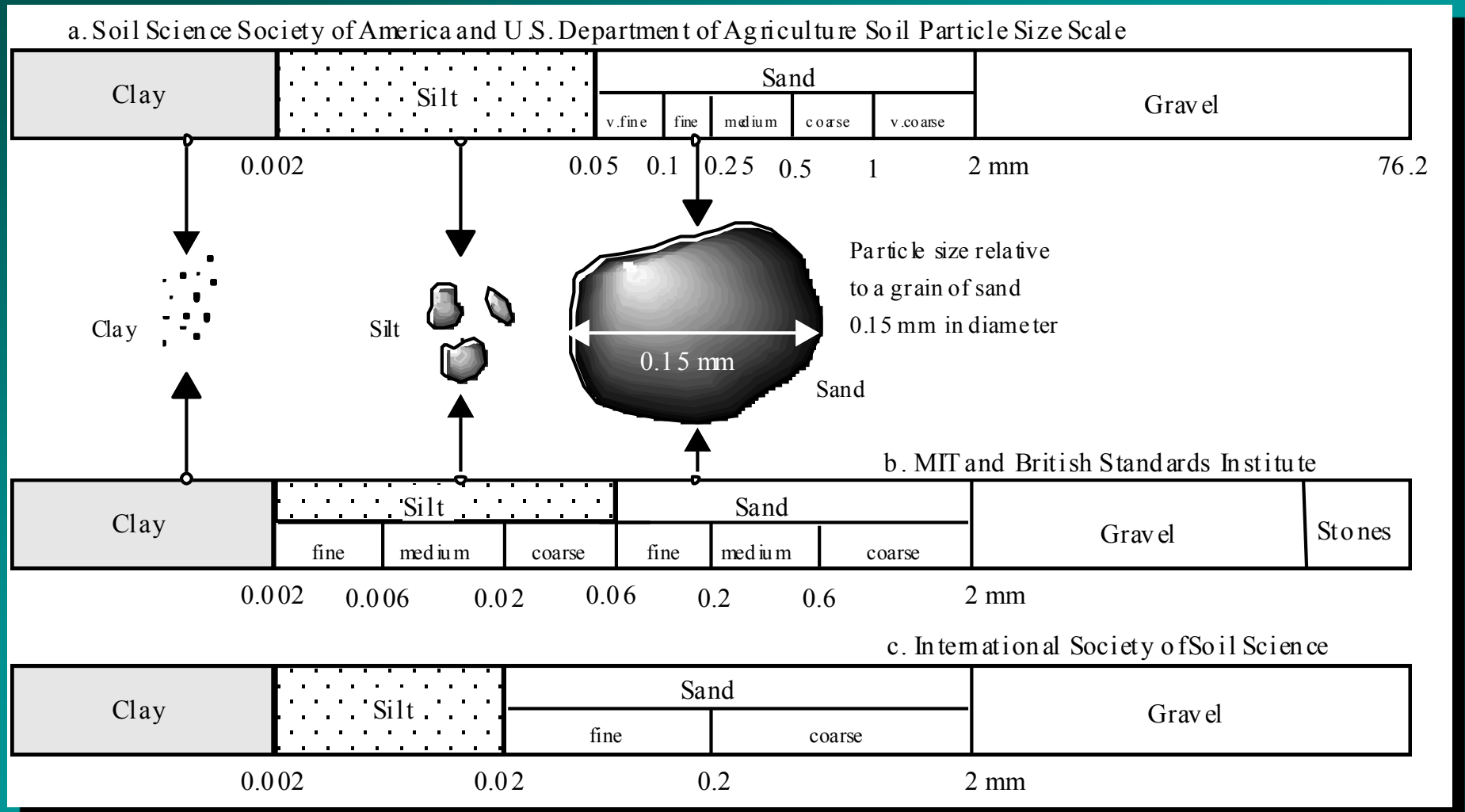

Jensen, 2000

Soil Texture Triangle

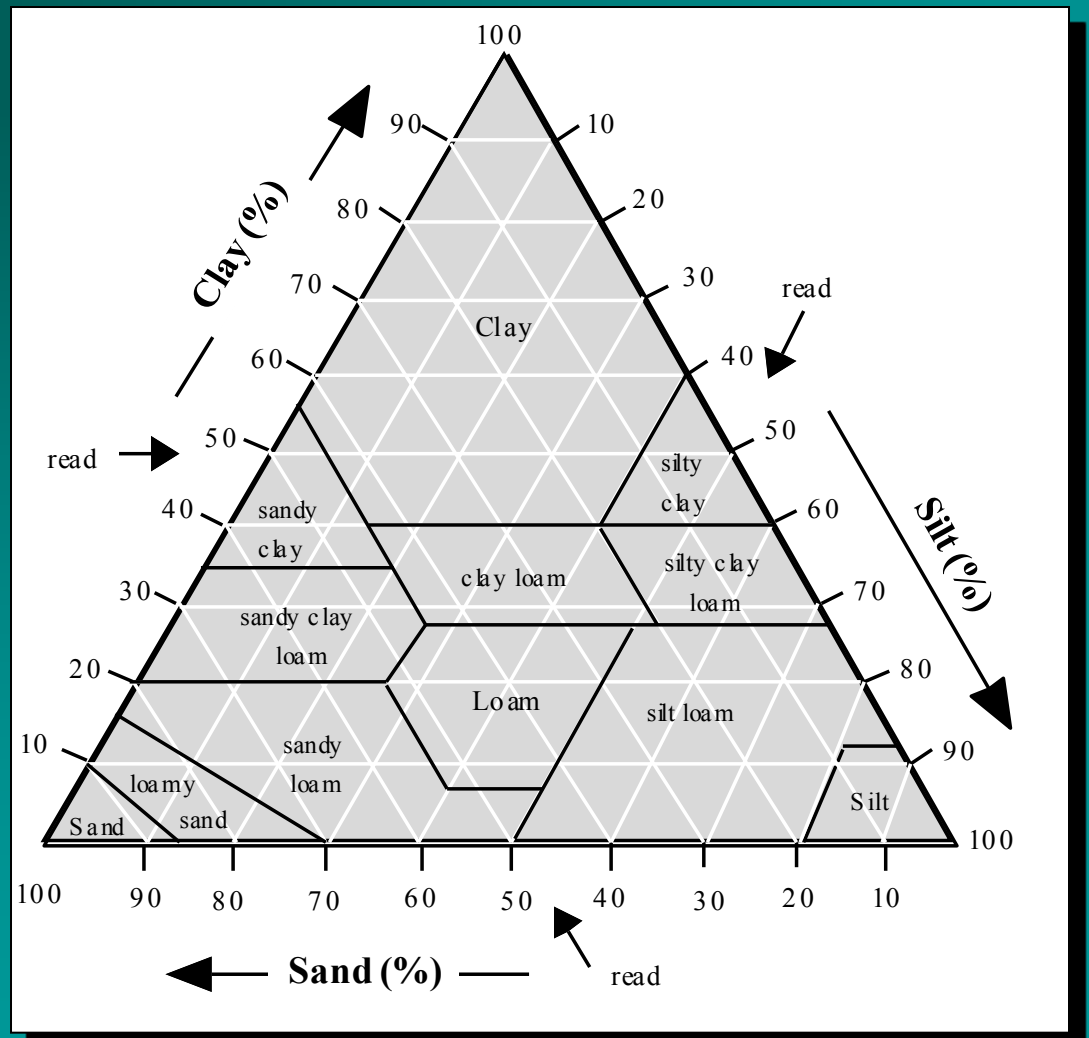

Jensen, 2000

Total Upwelling Radiance (L_t) Recorded by a Remote Sensing System over Exposed Soil is a Function of Electromagnetic Energy from Several Sources

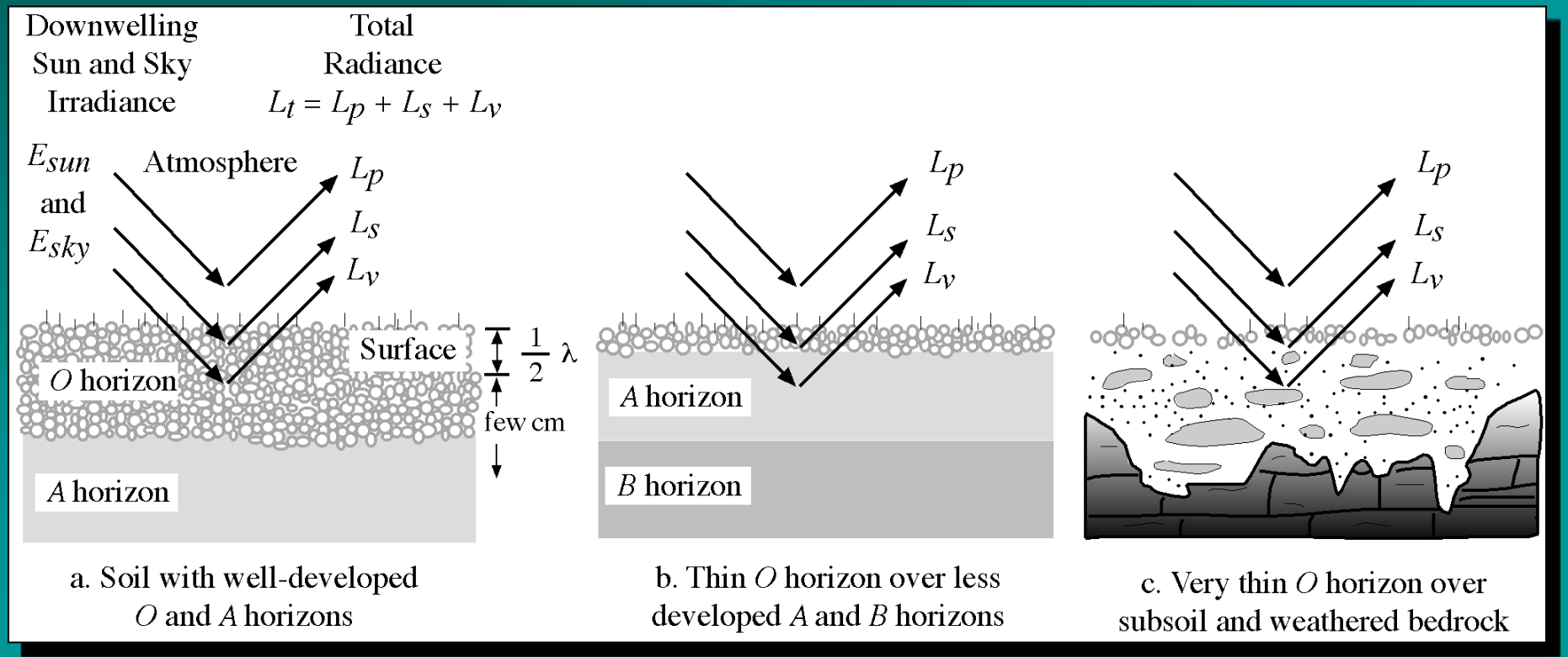

Jensen, 2000

Spectral Reflectance Characteristics of *Soils* Are a Function of Several Important Characteristics

- soil texture (percentage of sand, silt, and clay),
- soil moisture content (e.g. dry, moist, saturated),
- organic matter content,
- iron-oxide content, and
- surface roughness.

Jensen, 2000

In situ Spectroradiometer Reflectance Curves for Dry Silt and Sand Soils

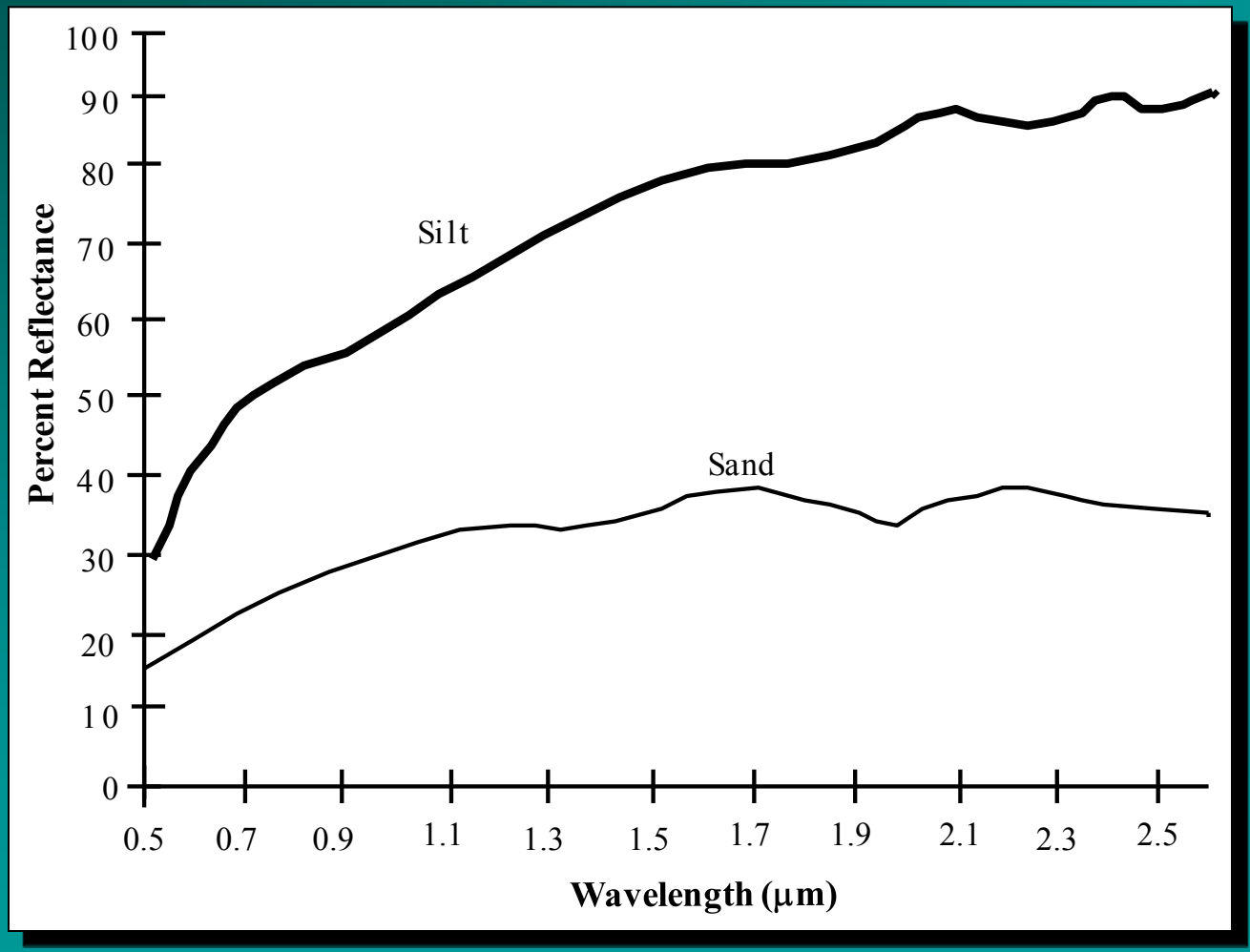

Jensen, 2000

Reflectance from Dry versus Wet Soils

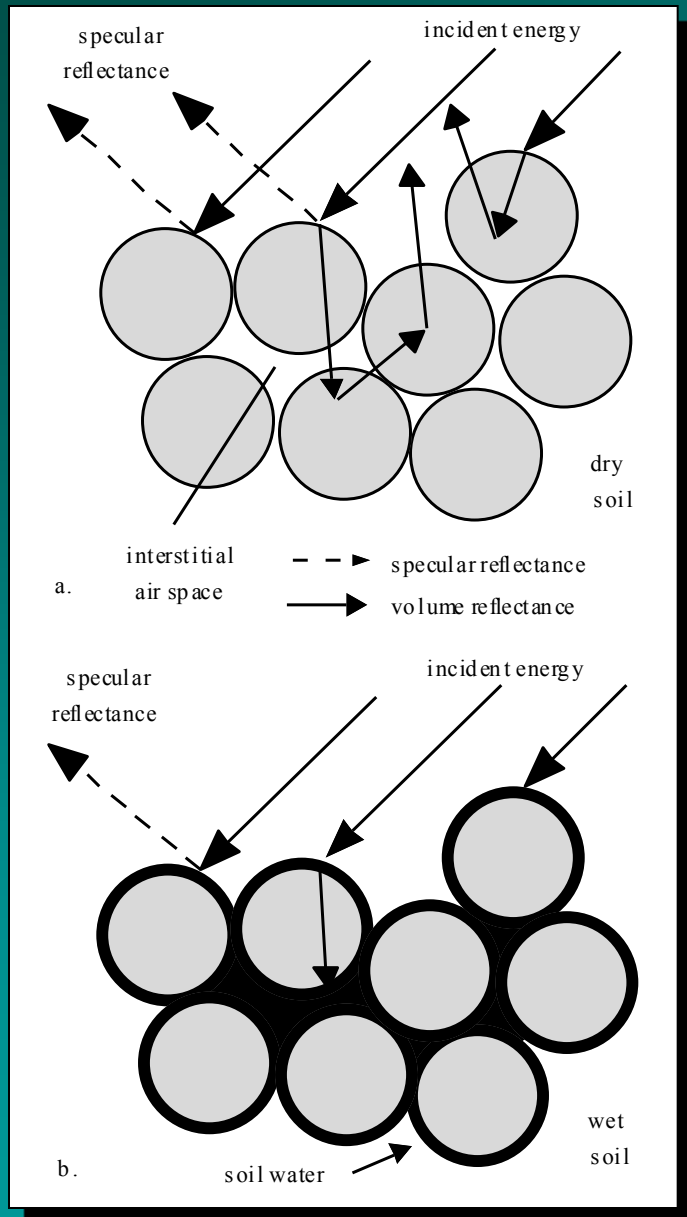

Jensen, 2000

Radiant energy may be reflected from the surface of the dry soil, or it penetrates into the soil particles, where it may be absorbed or scattered. Total reflectance from the dry soil is a function of specular reflectance and the internal volume reflectance.

As soil moisture increases, each soil particle may be encapsulated with a thin membrane of capillary water. The interstitial spaces may also fill with water. The greater the amount of water in the soil, the greater the absorption of incident energy and the lower the soil reflectance.

Reflectance from Moist Sand and Clay Soils

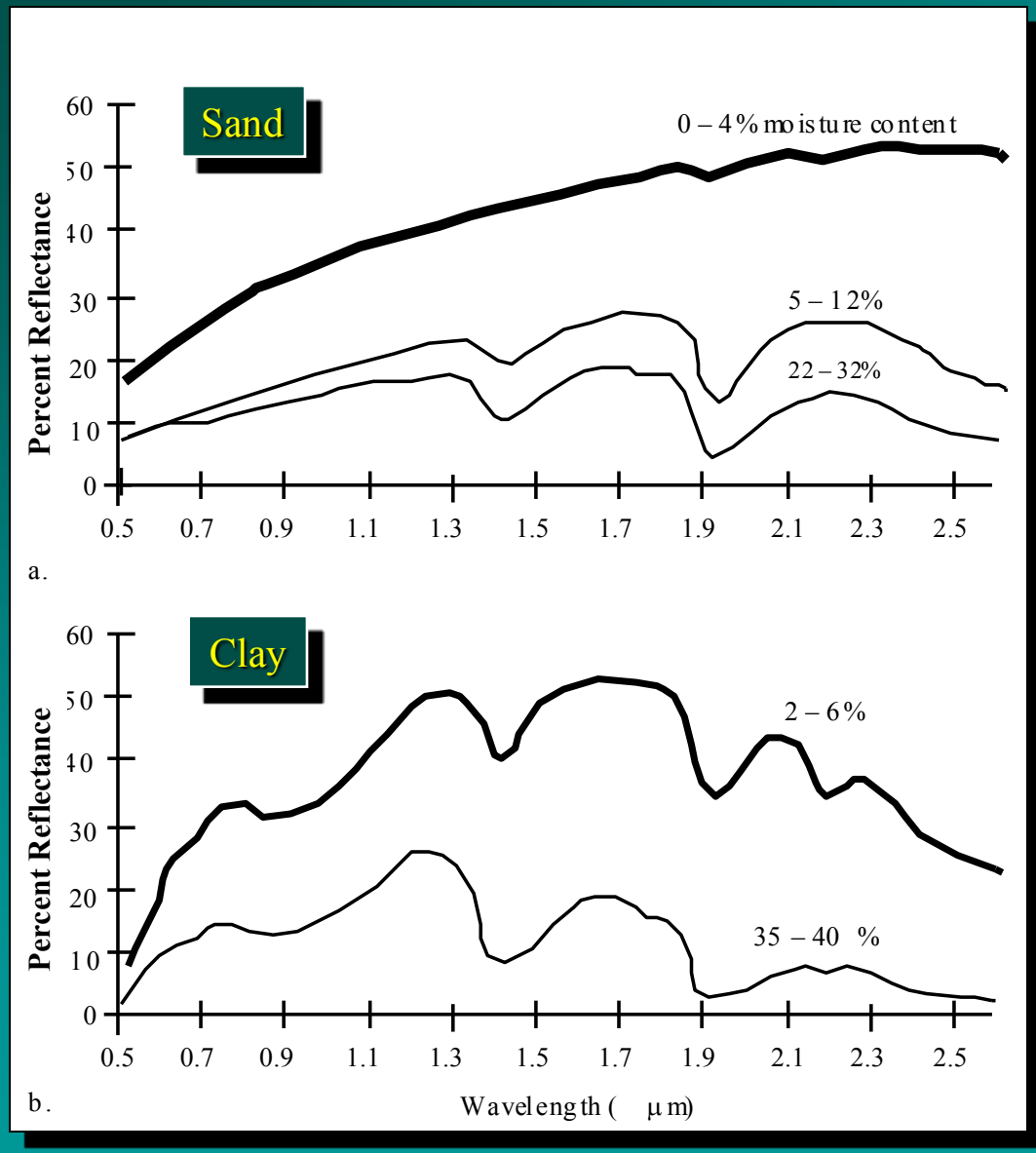

Higher moisture content in (a) sandy soil, and (b) clayey soil results in decreased reflectance throughout the visible and near-infrared region, especially in the water-absorption bands at 1.4, 1.9, and 2.7 µm.

Jensen, 2000

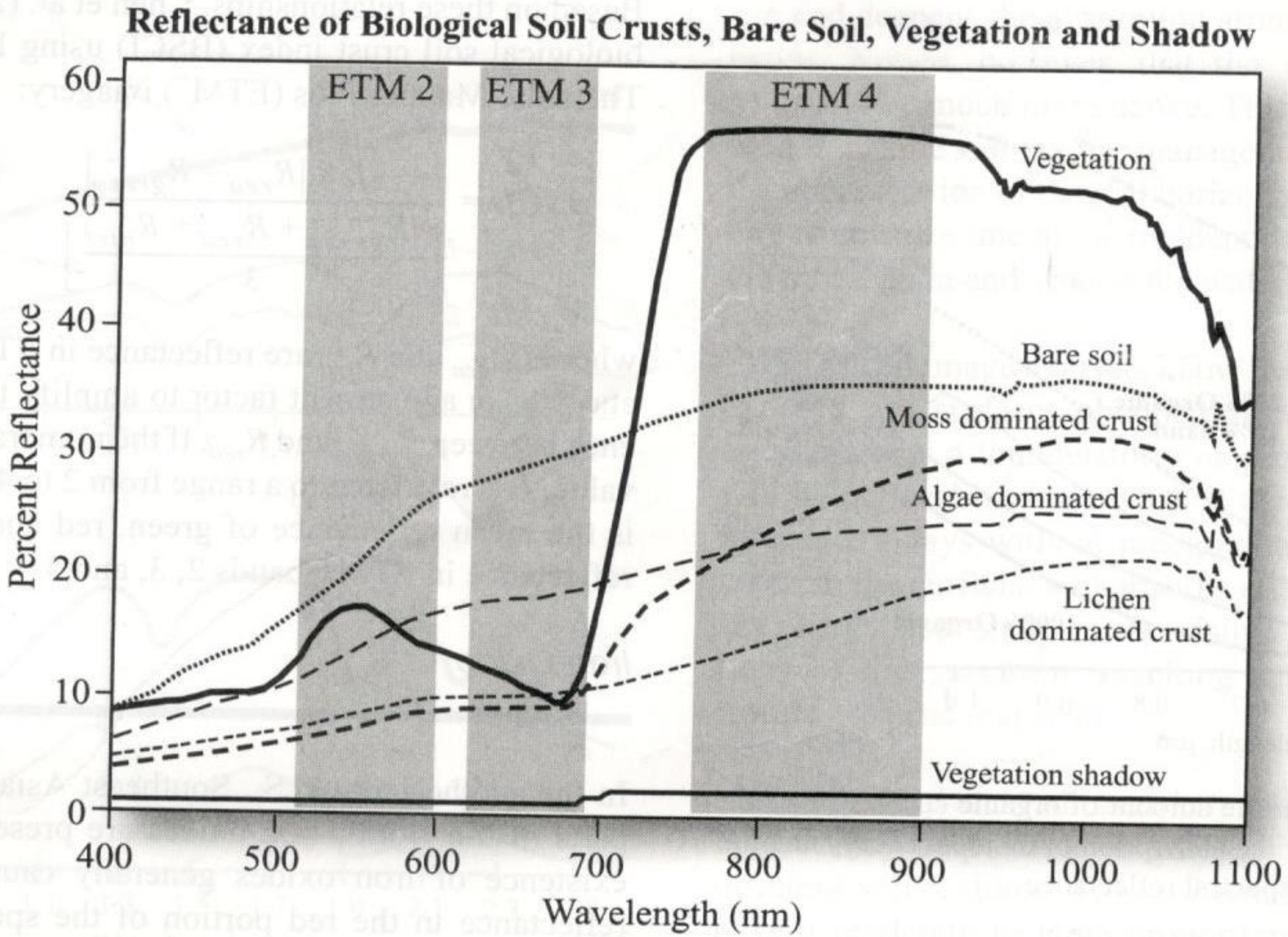

Figure 14-10 Spectral reflectance of biological soil crusts compared with bare soil, vegetation, and vegetation shadow refle
al., 2000; reprinted with permission from Elsevier).

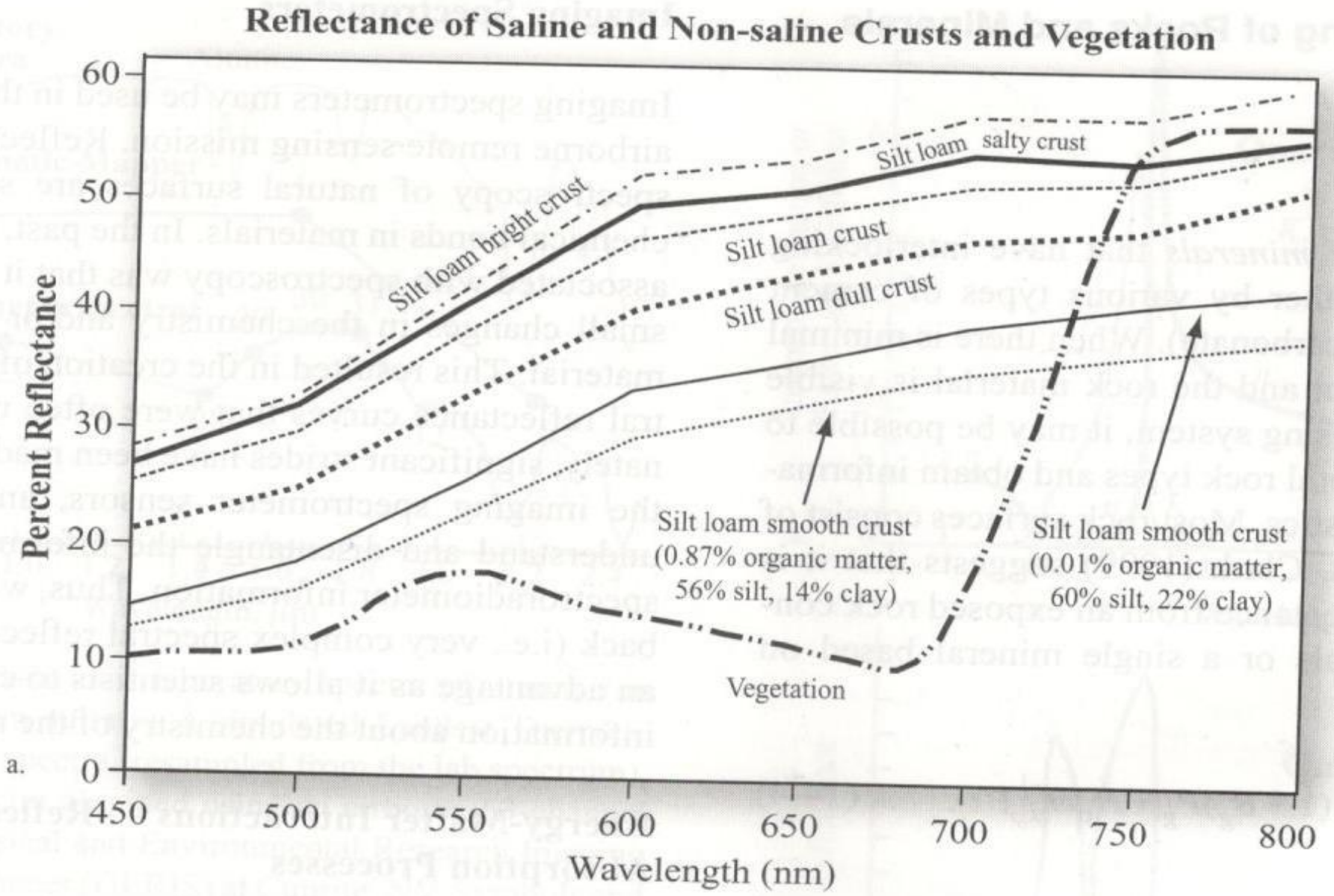
Reflectance of Saline and Non-saline Crusts and Vegetation
Percent Reflectance
60
50
40
30
20
10
0
450
500
550
600
650
700
750
800
Wavelength (nm)
Silt loam bright crust
Silt loam salty crust
Silt loam crust
Silt loam dull crust
Silt loam smooth crust
(0.87% organic matter,
56% silt, 14% clay)
Silt loam smooth crust
(0.01% organic matter,
60% silt, 22% clay)
Vegetation
a.

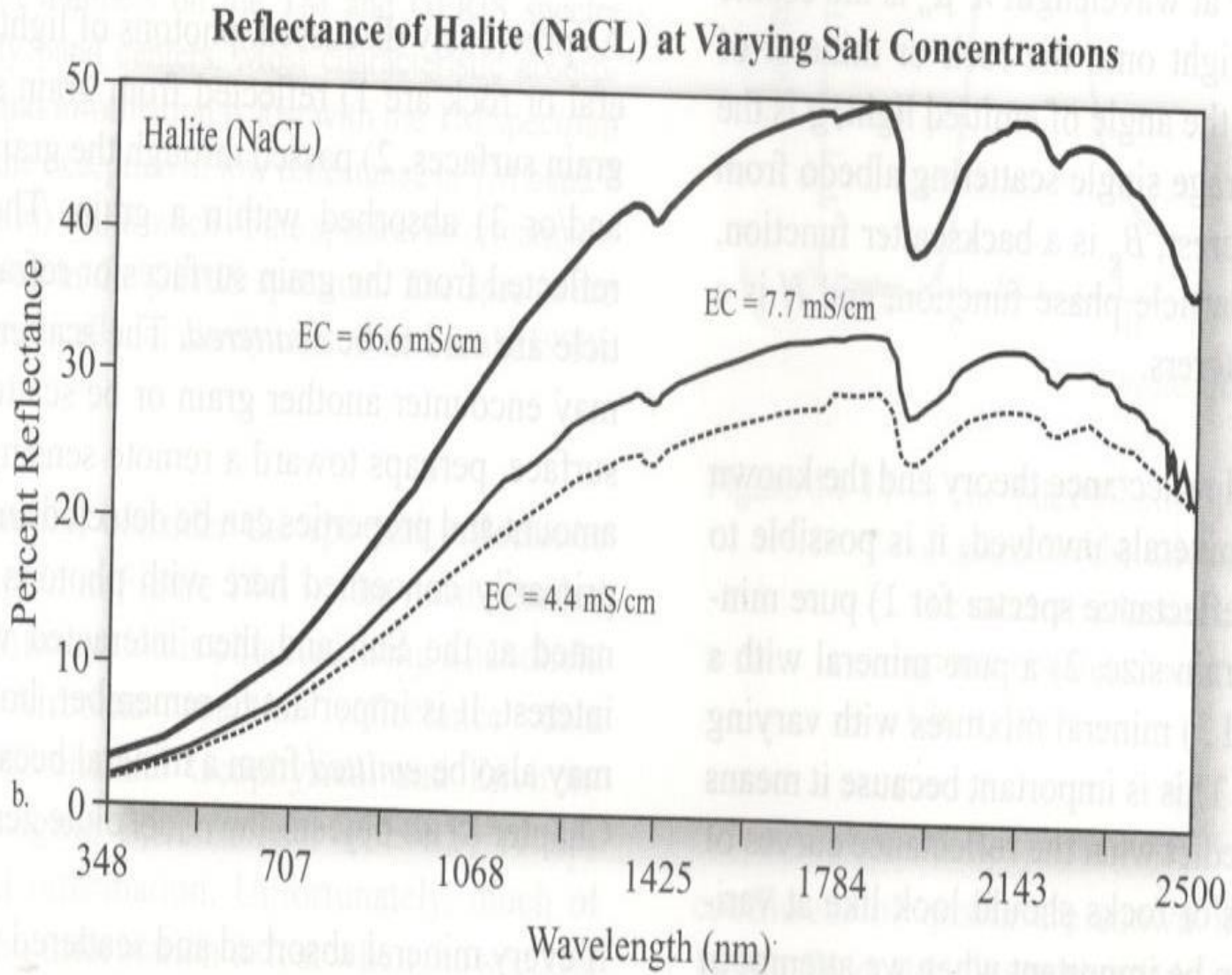

14-12 a) Spectral reflectance of saline and non-saline soil crusts (Metternicht and Zinck, 2003; reprinted with permission from Elsevier) versus the spectral response of vegetation. b) Spectroradiometer reflectance measurements of halite (NaCL) at varying salt concentrations (Farifteh et al., 2006; reprinted with permission from Elsevier).

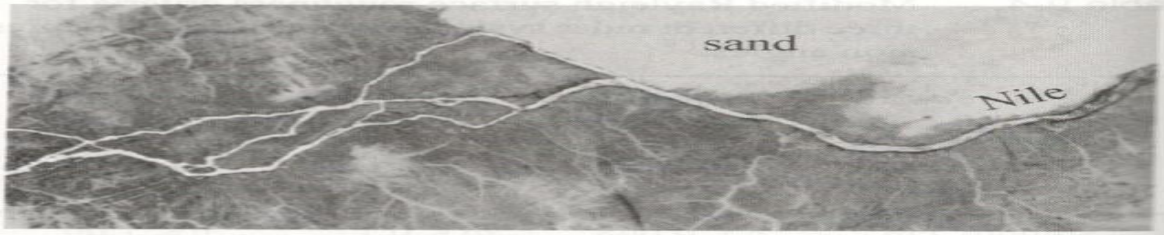

a. Shuttle photograph.

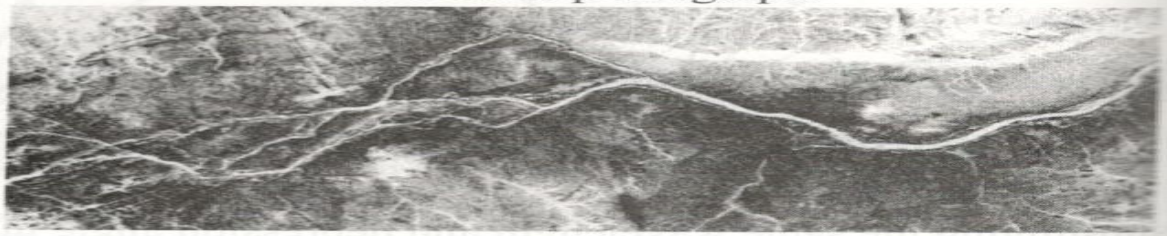

b. SIR-C C-band HV.

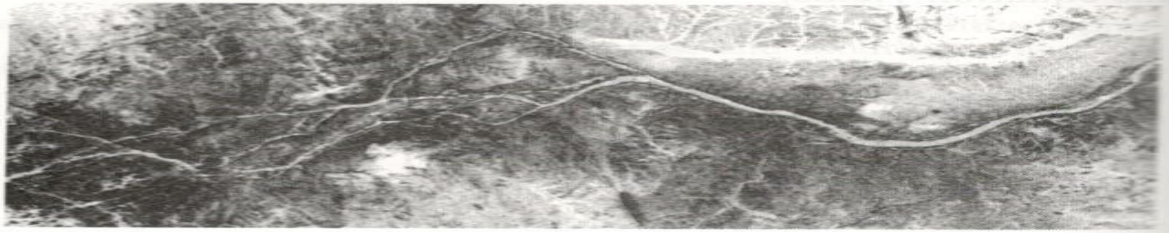

c. SIR-C L-band HV.

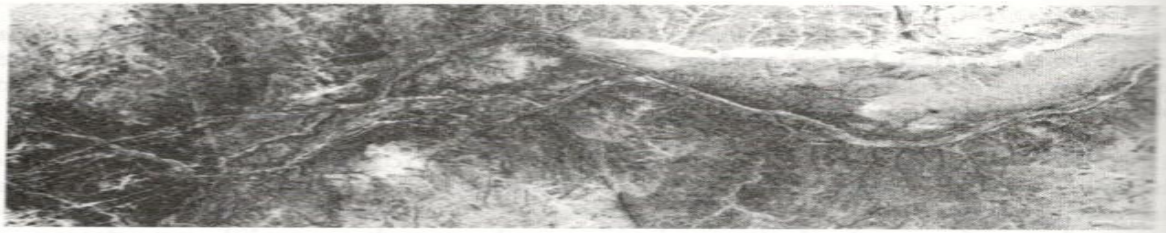

d. SIR-C L-band HH.

Figure 9-21 Example of radar penetration of dry soil along the Nile River, Sudan. a) Black-and-white version of a color-infrared photograph acquired by Space Shuttle *Columbia* crew in November 1995; b–d) SIR-C/X-SAR images acquired by the Space Shuttle *Endeavor* in April 1994. Subtle, different information is recorded in each of the three radar images. Each reveals an ancient, previously unknown channel of the Nile. Radar brightness values are inverted in these examples (courtesy Jet Propulsion Lab).

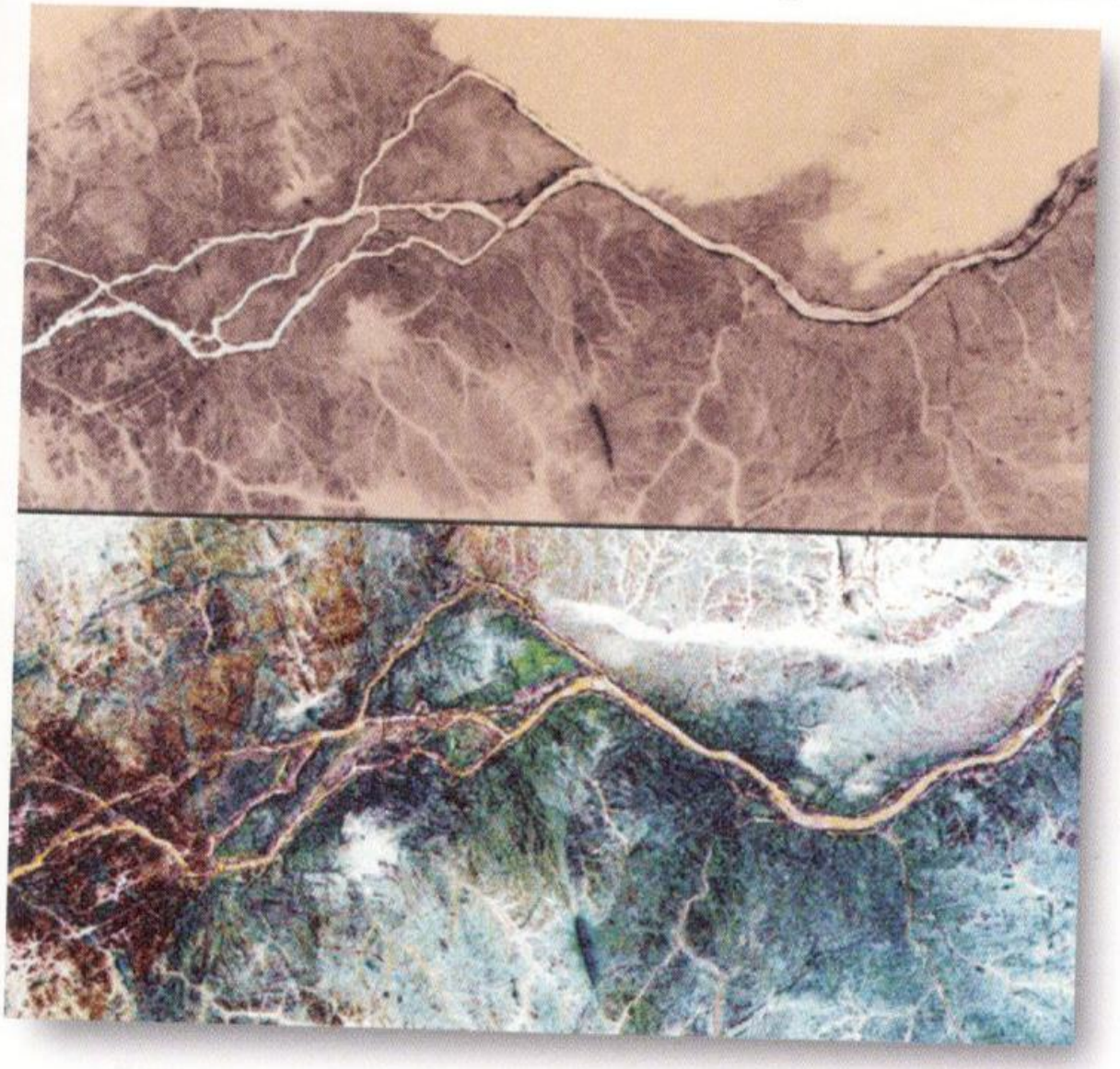

a. Space Shuttle photograph.

b. SIR-C/X-SAR image.

ace Shuttle photograph of the Nile River, Sudan. b) SIR-C/X-SAR color-composite image of C-band with HV polar
n, L-band with HV polarization, and L-band with HH polarization. The data were acquired by the Space Shuttle *En*
r in April, 1994 (courtesy NASA Jet Propulsion Lab).

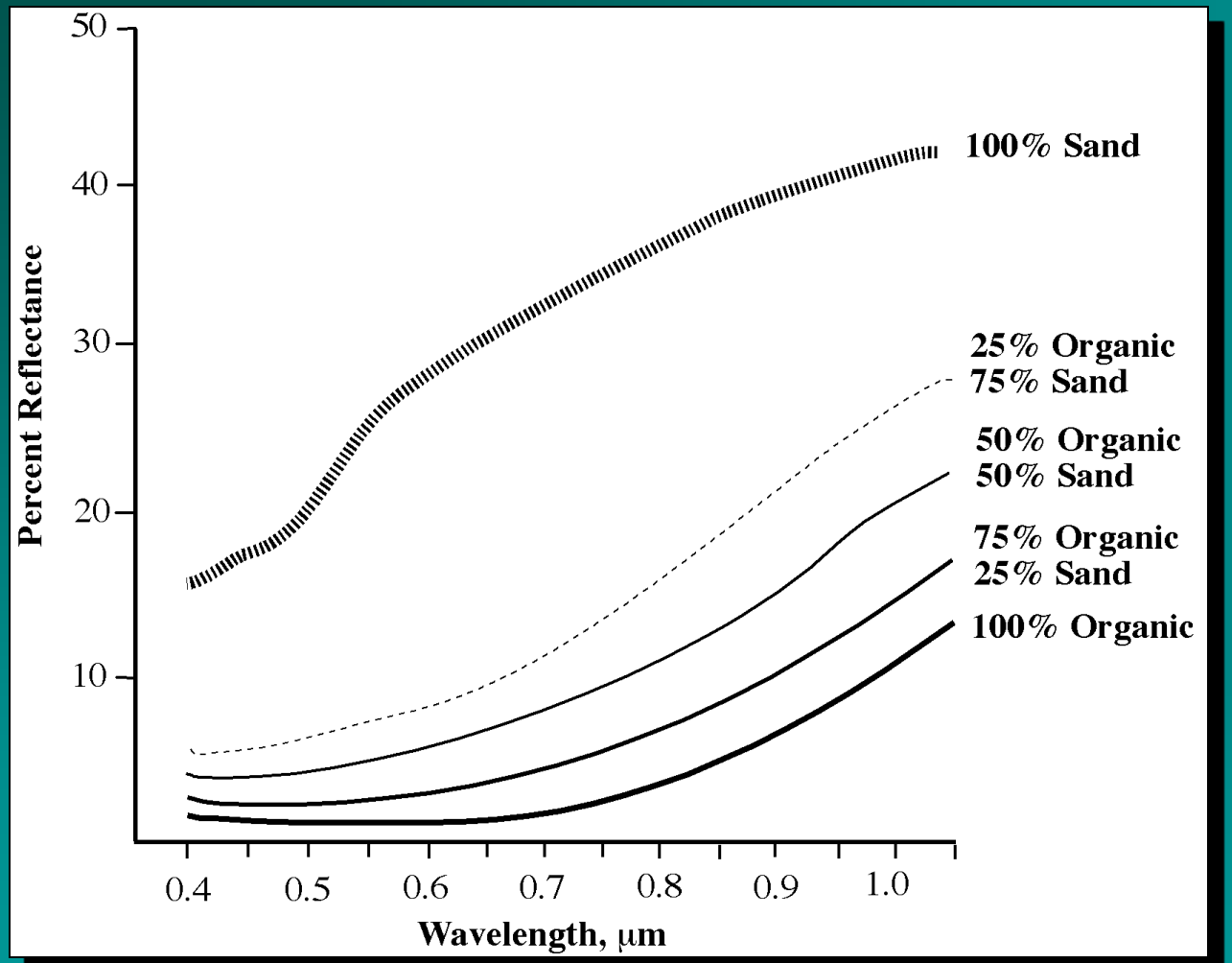

Organic Matter in a Sandy Soil

Generally, the greater the amount of organic content in a soil, the greater the absorption of incident energy and the lower the spectral reflectance

Jensen, 2000

Iron Oxide in a Sandy Loam Soil

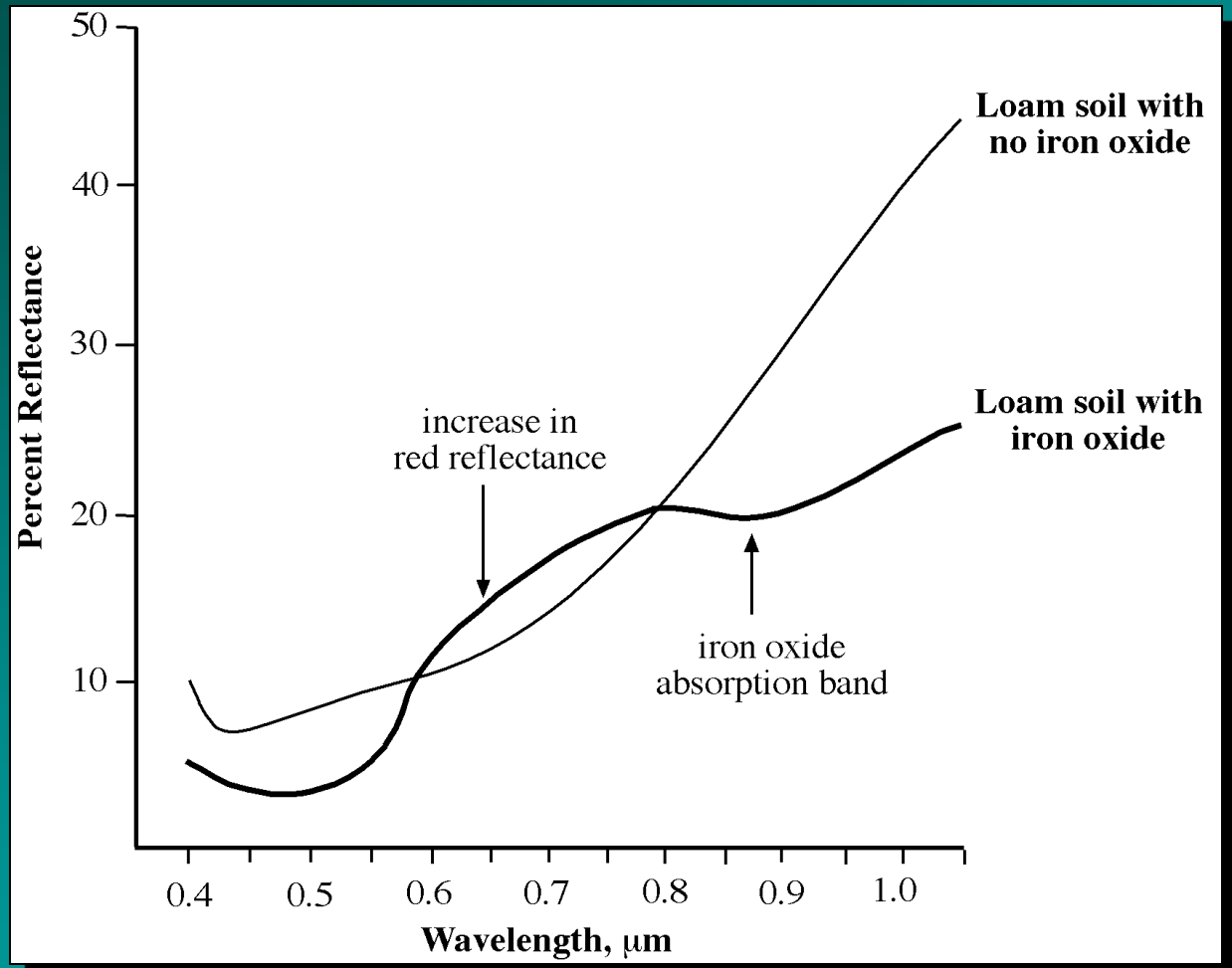

Jensen, 2000

Iron oxide in a sandy loam soil causes an increase in reflectance in the red portion of the spectrum (0.6 - 0.7 μm) and a decrease in in near-infrared (0.85 - 0.90 μm) reflectance

Remote Sensing of Rock and Minerals

Remote Sensing of Soils, Minerals, and Geomorphology

• *Rocks* are assemblages of minerals that have interlocking grains or are bound together by various types of cement (usually silica or calcium carbonate). When there is minimal vegetation and soil present and the rock material is visible directly by the remote sensing system, it maybe possible to differentiate between several rock types and obtain information about their characteristics using remote sensing techniques. Most rock surfaces consist of several types of minerals.

Jensen, 2000

Remote Sensing of Rocks and Minerals

Clark (1999) suggests that it is possible to model the reflectance from an exposed rock consisting of several minerals or a single mineral based on Hapke's (1993) equation:

$$r_\lambda = [[(w'/4_\pi) \text{ x } (\mu / \mu + \mu_o)] \text{ x } [(1+B_g)P_g + H\,\mu H\,\mu_o^{-1}]$$

Where r_λ is the reflectance at wavelength λ, u_o is the cosine of the angle of incident light onto the rock or mineral of interest, μ is the cosine of the angle of emitted light, g is the phase angle, w' is the average single scattering albedo from the rock or mineral of interest, B_g is a back-scattering function, P_g is the average single particle phase function, and H is a function for isotropic scatterers.

Remote Sensing of Rocks and Minerals Using Spectroradiometers

There are a number of processes that determine how a mineral will absorb or scatter the incident energy. Also, the processes absorb and scatter light differently depending on the wavelength (λ) of light being investigated. The variety of absorption processes (e.g., electronic and vibrational) and their wavelength dependence allow us to derive information about the chemistry of a mineral from its reflected or emitted energy. The ideal sensor to use is the *imaging spectrometer* because it can record much of the absorption information, much like using an *in situ* spectroradiometer.

All materials have a complex *index of refraction*. If we illuminate a plane surface with photons of light from directly overhead, the light (R), will be reflected from the surface according to the Fresnel equation:

$$R = [(n - 1)^2 + K^2]/ [(n + 1)^2 + K^2]$$

where n is the index of refraction, and K is the extinction coefficient.

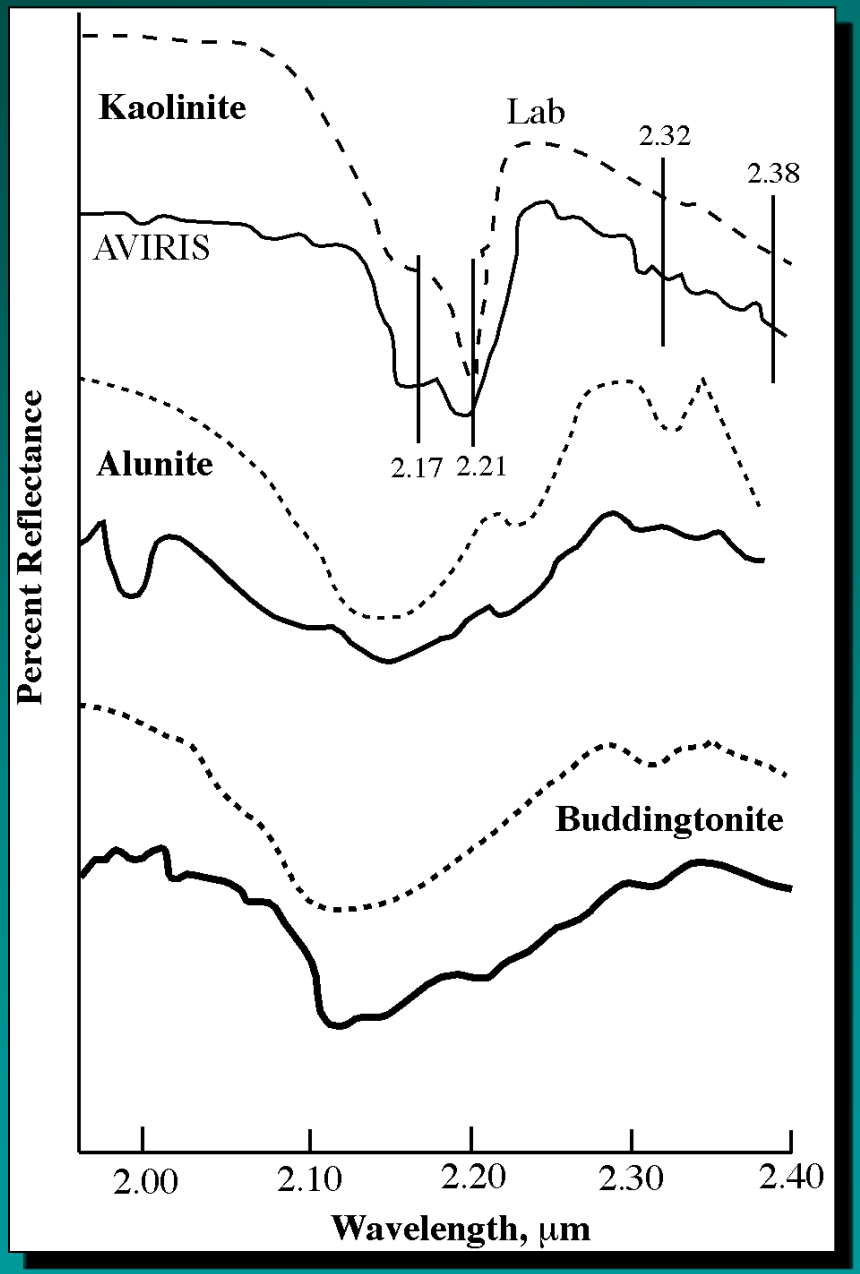

Spectra of Three Minerals Derived from NASA's Airborne Visible Infrared Imaging Spectrometer (AVIRIS) and as Measured Using A Laboratory Spectroradiometer (after Van der Meer, 1994)

Jensen, 2000

Alunite Laboratory Spectra, Simulated Landsat Thematic Mapper Spectra, and Spectra from a 63-Channel GERIS Instrument over Cuprite, Nevada

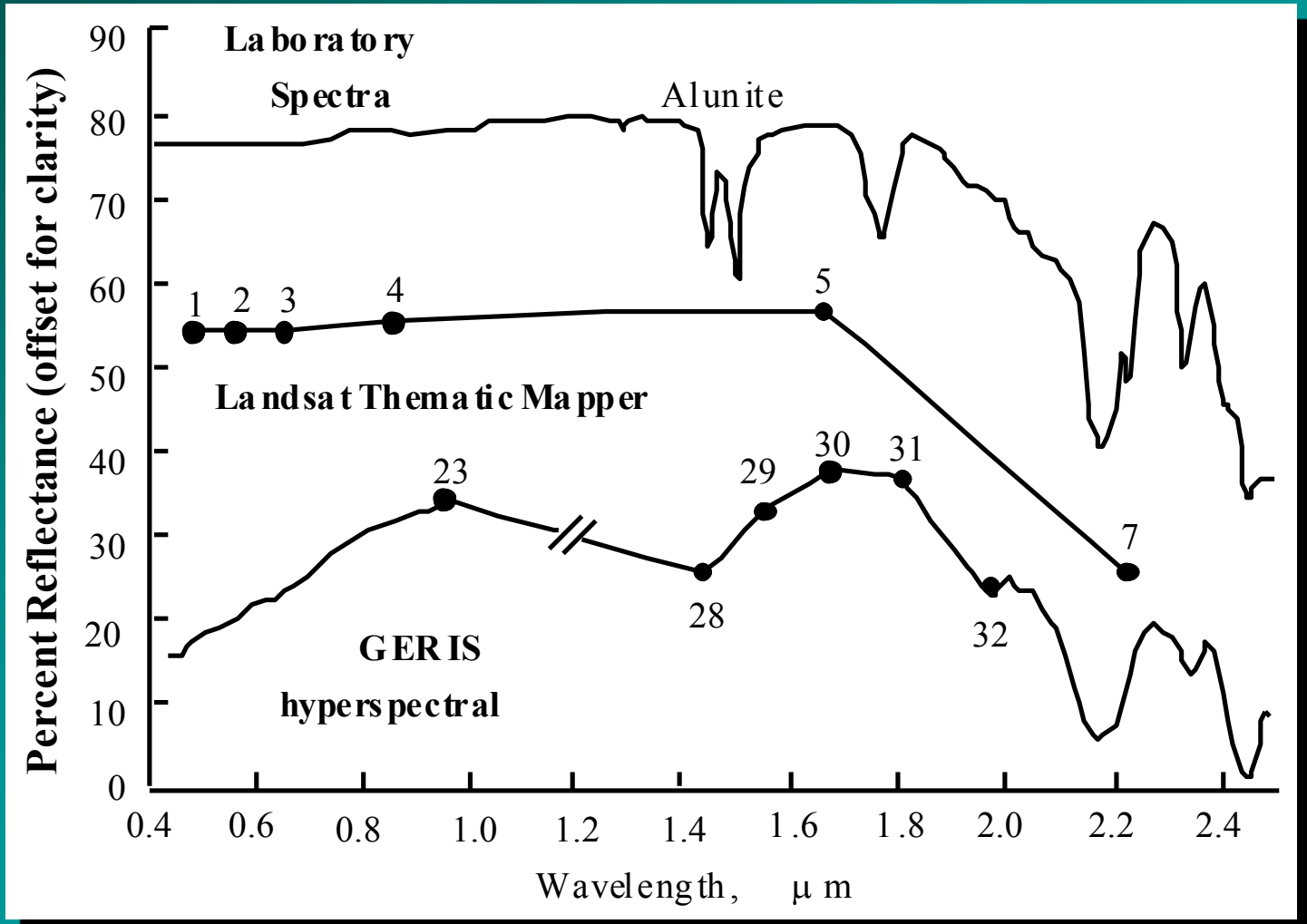

Jensen, 2000

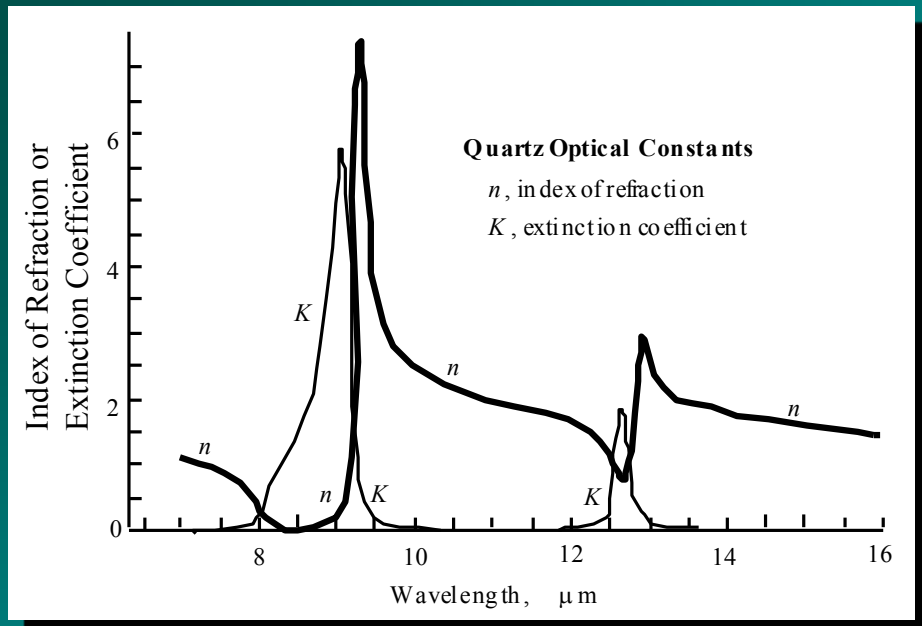

Index of refraction and extinction coefficient of quartz for the wavelength interval 6-16 µm

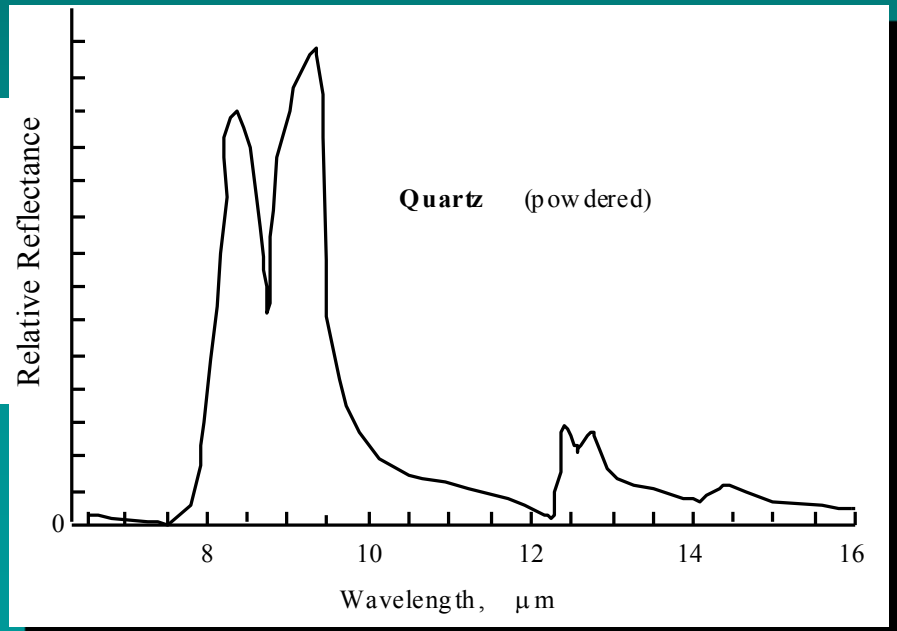

Spectral reflectance characteristics of powdered quartz obtained using a spectroradiometer (after Clark, 1999)

Jensen, 2000

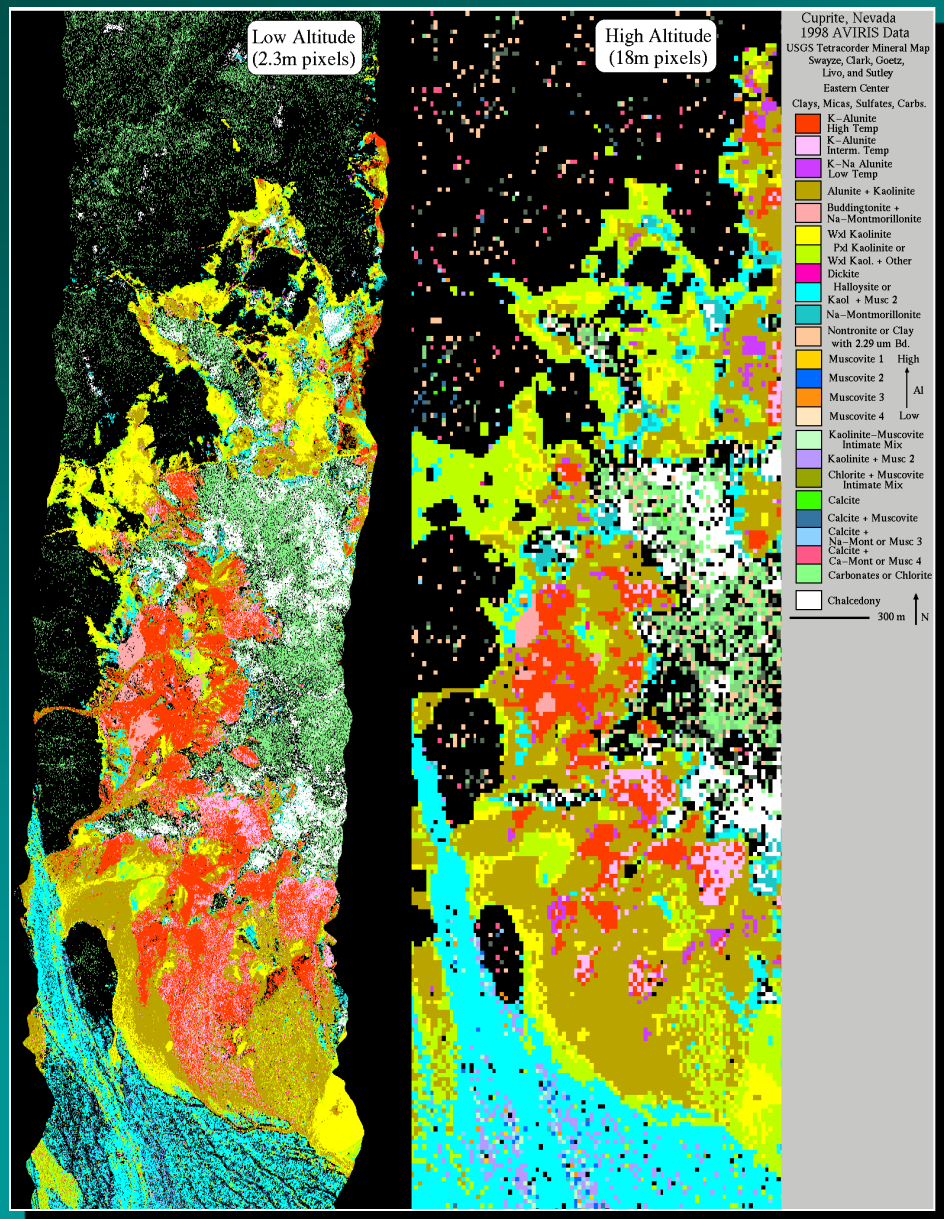

Mineral Maps of Cuprite, NV, Derived from Low Altitude (3.9 km AGL) and High Altitude (20 km AGL) AVIRIS Data obtained on October 11 and June 18, 1998

Hyperspectral data were analyzed using the USGS Tetracorder program.

Remote Sensing of Geology and Geomorphology

Remote Sensing of Geology and and Geomorphology

Geologists often use remote sensing in conjunction with *in situ* observation to identify the *lithology* of a rock type, i.e., its origin. The different rock types are formed by one of three processes;

- igneous rocks are formed from moulten material;
- sedimentary rocks are formed from the deposition of particles of pre-existing rocks and plant and animal remains; or
- metamorphic rocks are formed by applying heat and pressure to previously existing rock.

Jensen, 2000

Rock Structure: Folding and Faulting

The type of rock determines how much differential stress (or compression) it can withstand. When a rock is subjected to compression, it may experience:

1) *elastic deformation* in which case it may return to its original shape and size after the stress is removed,

2) *plastic deformation* of rock called *folding*, which is irreversible (i.e., the compressional stress is beyond the elastic limit, and/or

3) *fracturing* where the plastic limit is exceeded and the rock breaks into pieces (the pieces can be extremely large!). This may result in *faulting*.

Jensen, 2000

Rock Structure: Folding

Folding takes place when horizontally bedded materials are compressed. The compression results in wavelike undulations imposed on the strata. There are four basic types of folds:

- *monoclines* (a single fold on horizontally bedded material; like a rounded ramp),
- *anticlines* (archlike convex upfold domes - oldest rocks in the center),
- *synclines* (troughlike concave downfold - youngest rocks in the center),
- *overturned* (where the folds are on top of one another):

Jensen, 2000

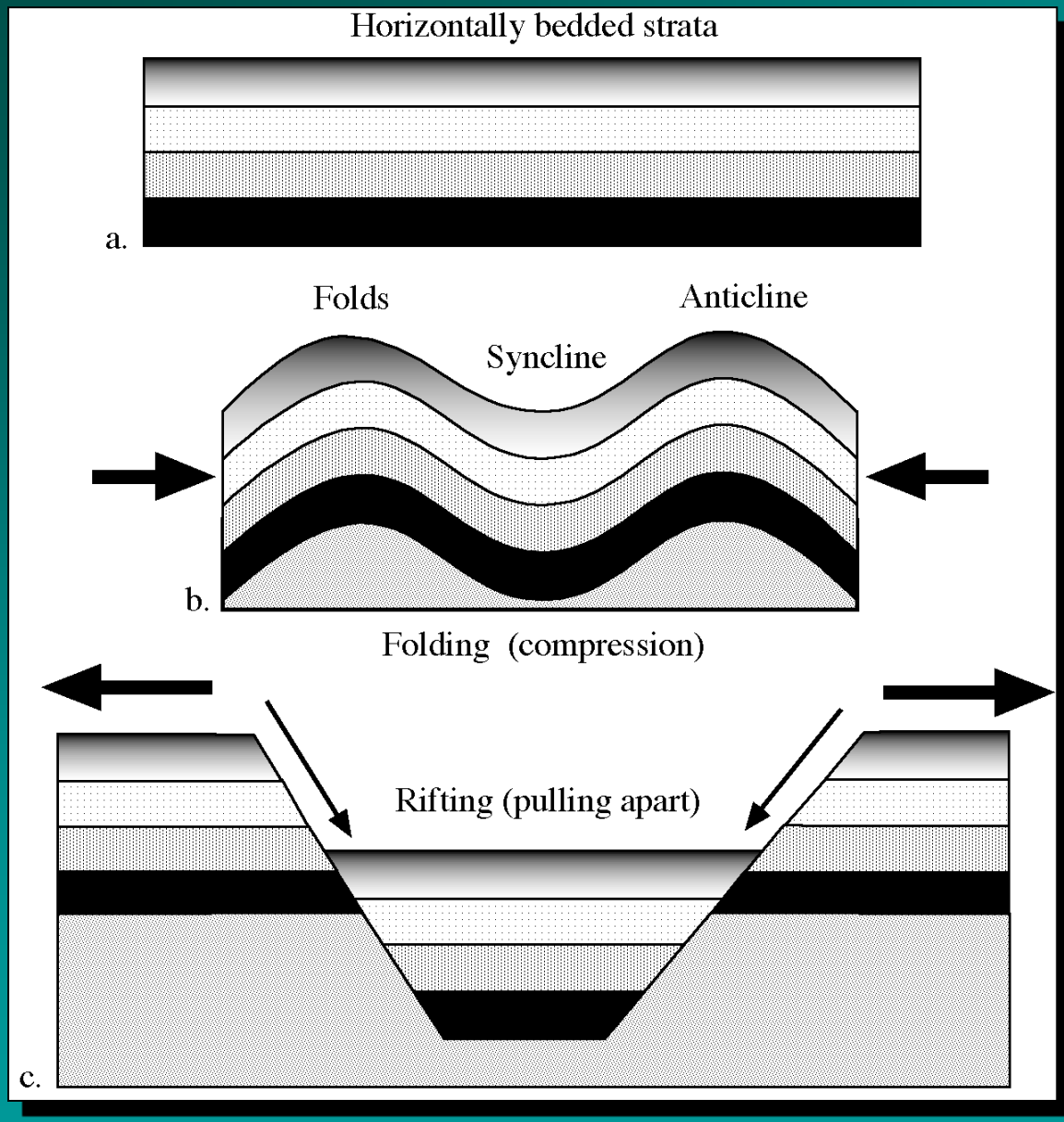

Effect of Folding (Compression) and Rifting (Pulling Apart) on Horizontally Bedded Strata

Jensen, 2000

Types of Folds Found on Horizontally Bedded Terrain

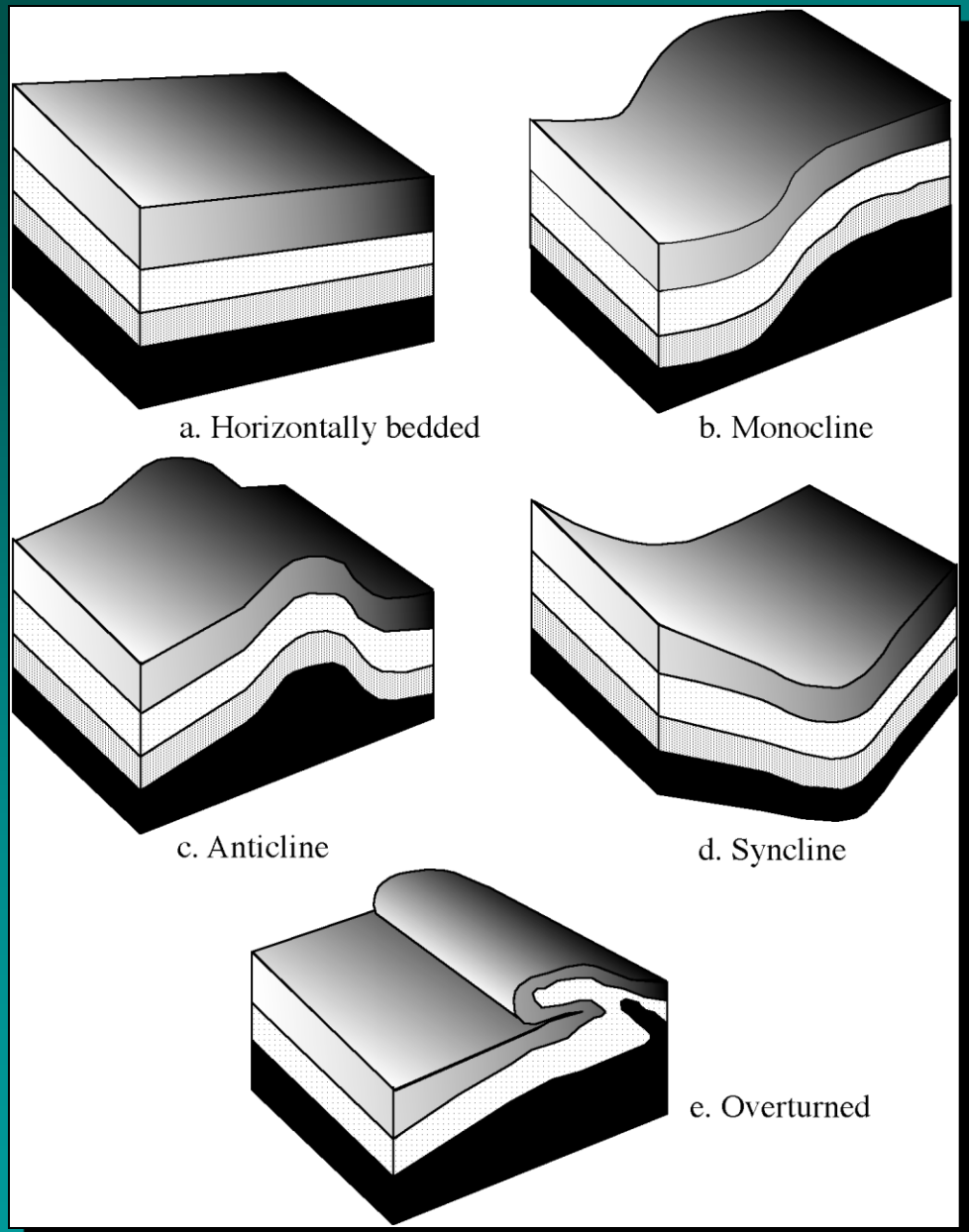

Jensen, 2000

Remote Sensing of Drainage Patterns

Remote Sensing of Drainage Density, Texture, and Pattern

Earth landscapes exhibit varying stream densities and patterns that can be identified using remote sensing data. *Drainage density* (D) is the total length (L) of n stream channels in a drainage basin divided by the basin surface area (A):

$$D = \frac{\sum_{1}^{n} L}{A}$$

The *permeability* of a soil or rock (i.e., how easily water passes through the material) has a great deal to do with drainage density. Permeability is inversely proportional to runoff. Where permeability is low and runoff is high, many gullies typically form. Conversely, when permeability is high and runoff is low, much of the water infiltrates into the ground and a larger surface area is required to provide sufficient runoff for the creation and maintenance of a channel (tributary). Weak impermeable clays and shales produce the highest drainage density. Regions with extremely high drainage density are called *badlands*.

Remote Sensing of Drainage Patterns

Drainage patterns developed through time on a landscape provide clues about bedrock lithology (e.g., igneous, sedimentary, metamorphic), topography (slope, aspect), the texture of the soil and/or bedrock materials, the permeability of the soil (how well water percolates through it), and the type of landform present (e.g,. alluvial, eolian, glacial. While *in situ* observations are essential, physical scientists often use the synoptic bird's-eye-view provided by remote sensing to appreciate regional drainage patterns, including:

- Dendritic
- Pinnate
- Trellis
- Rectangular
- Parallel
- Annular
- Dichotomic
- Braided
- Deranged
- Anastomotic
- Sinkhole (doline)
- Radial (Centrifugal) and Centripetal

Jensen, 2000

Drainage Patterns: Dendritic, Trellis, and Rectangular

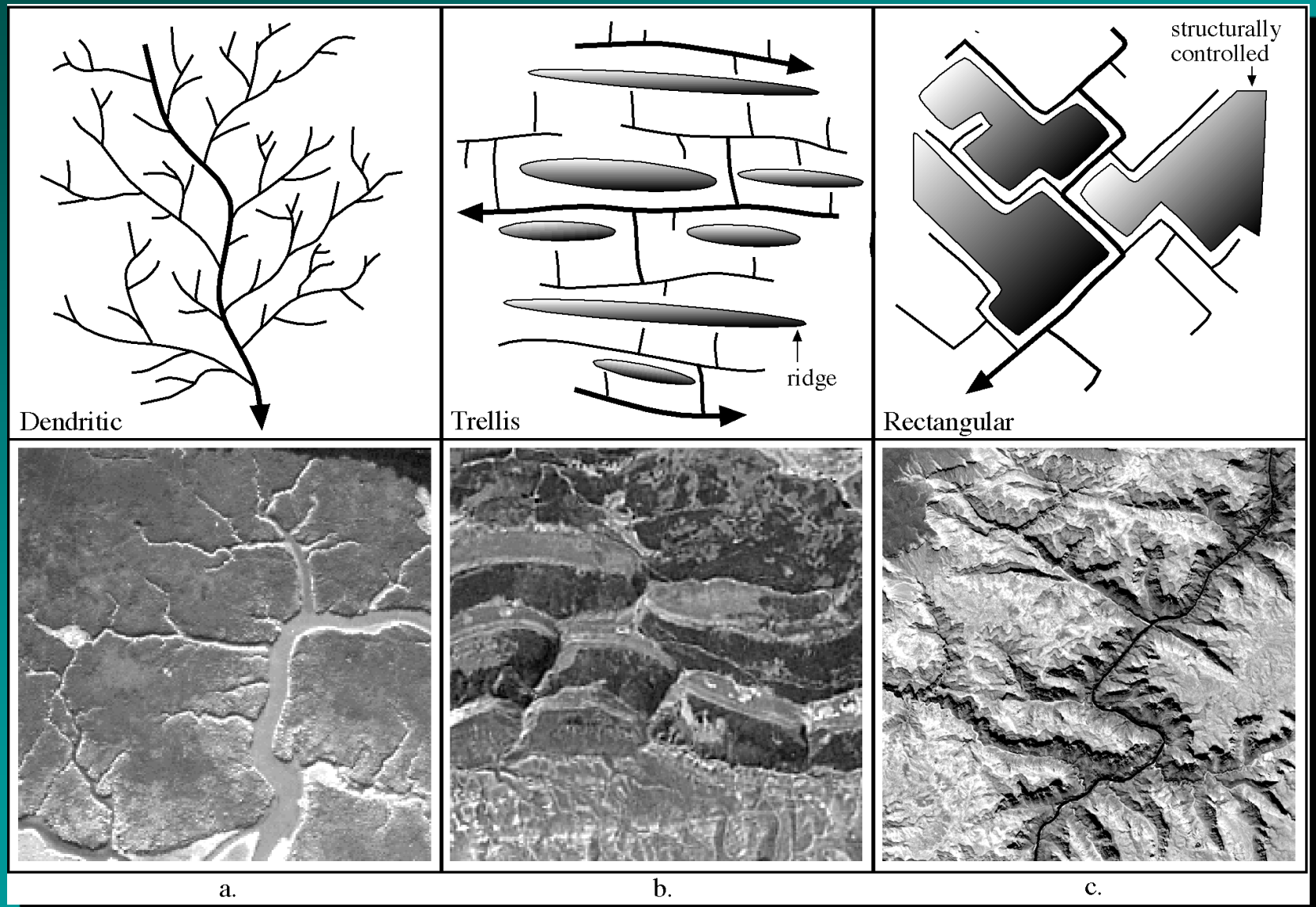

Jensen, 2000

Drainage Patterns: Parallel, Radial and Centripetal, Annular

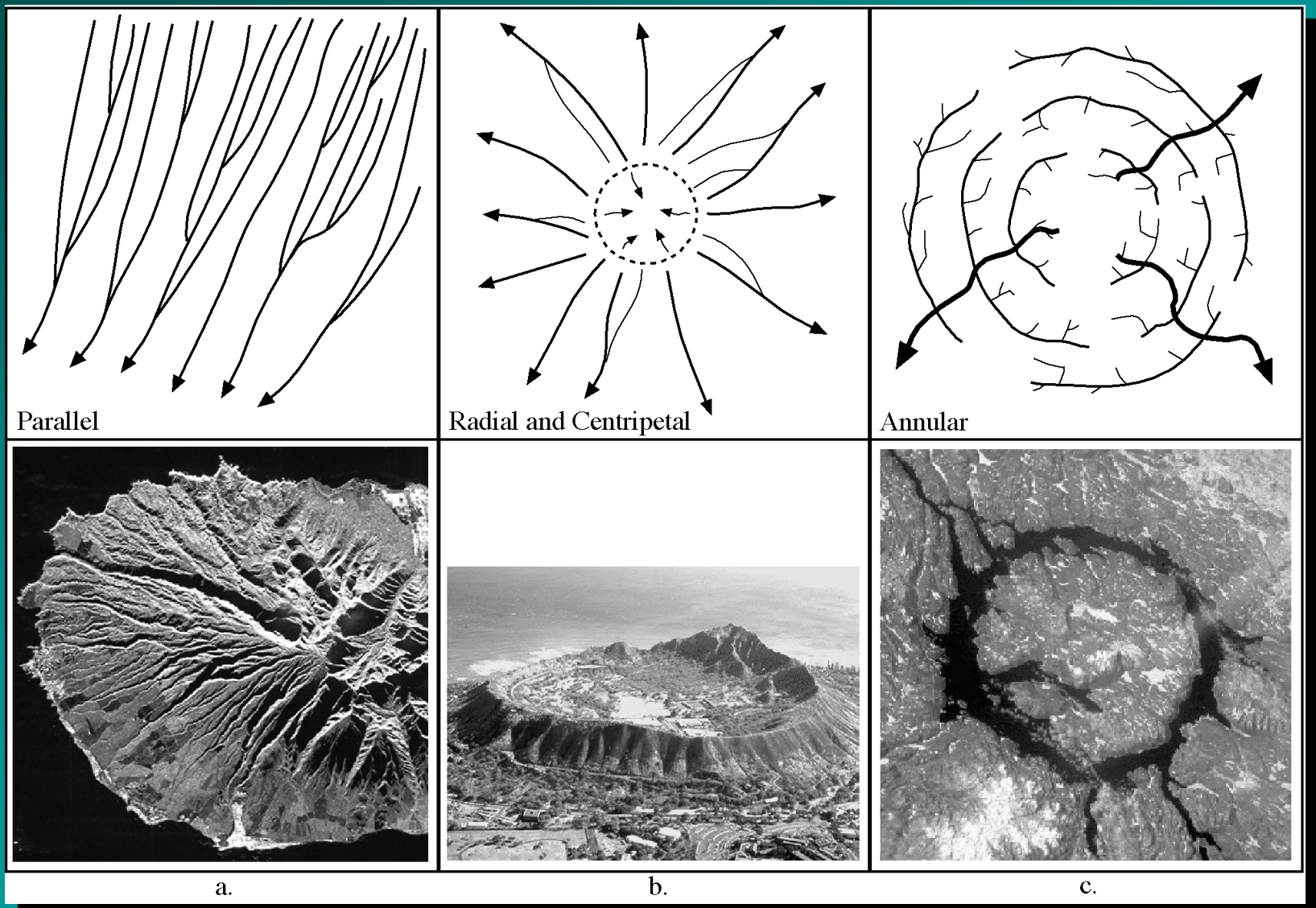

Jensen, 2000

Drainage Patterns: Dichotomic, Braided, and Anastomotic

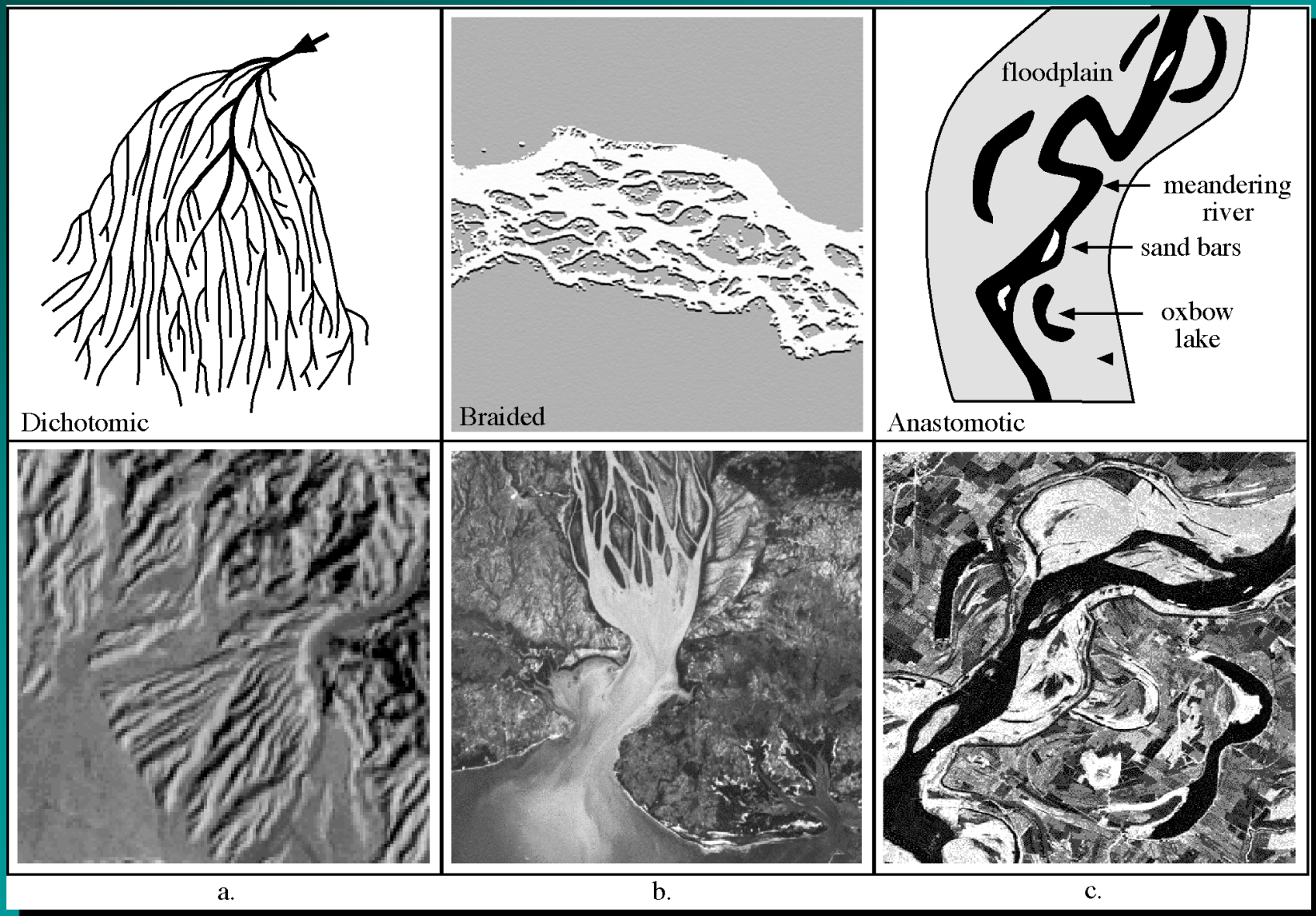

Jensen, 2000

Types of Faults

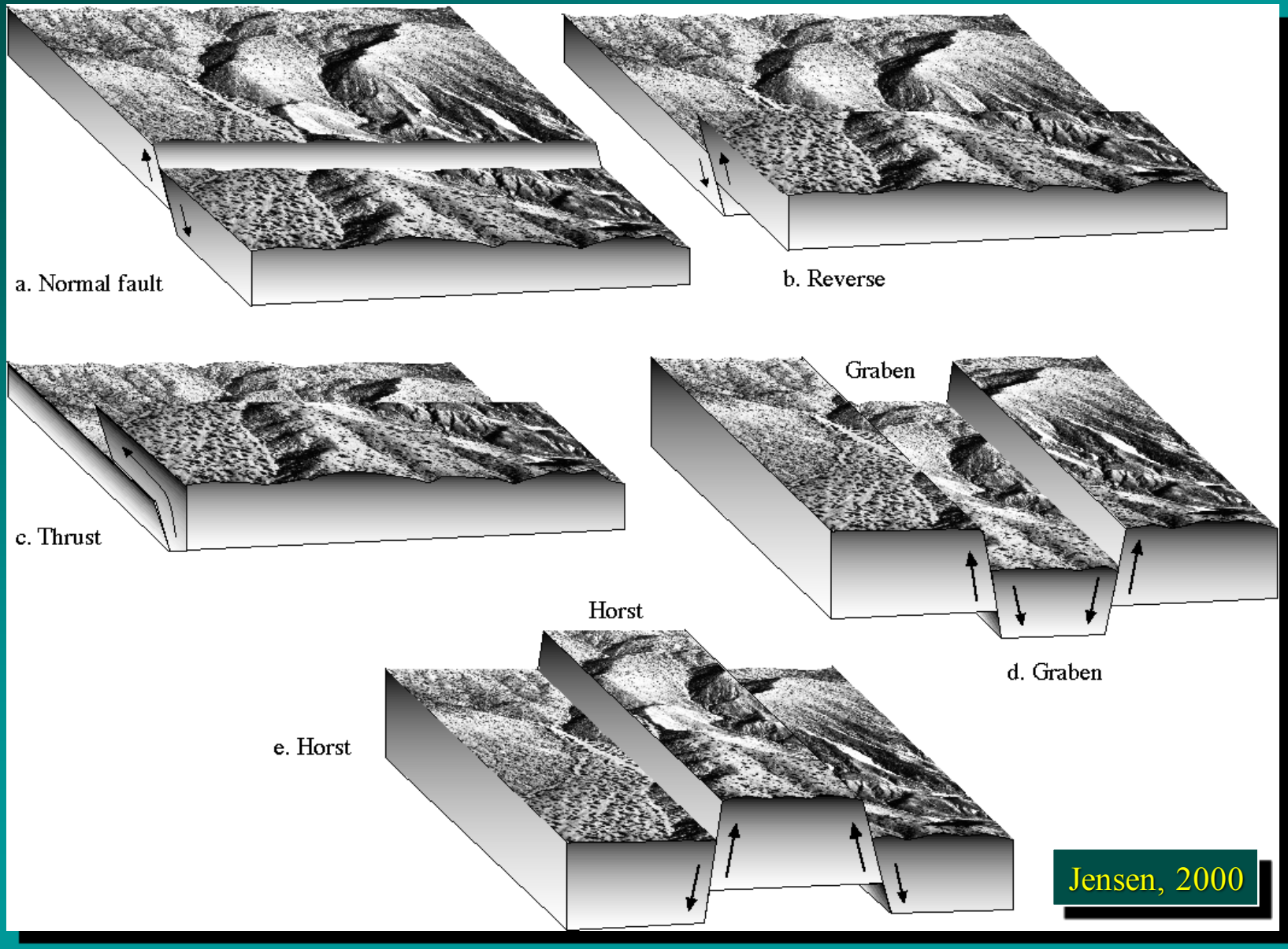

Fault Nomenclature

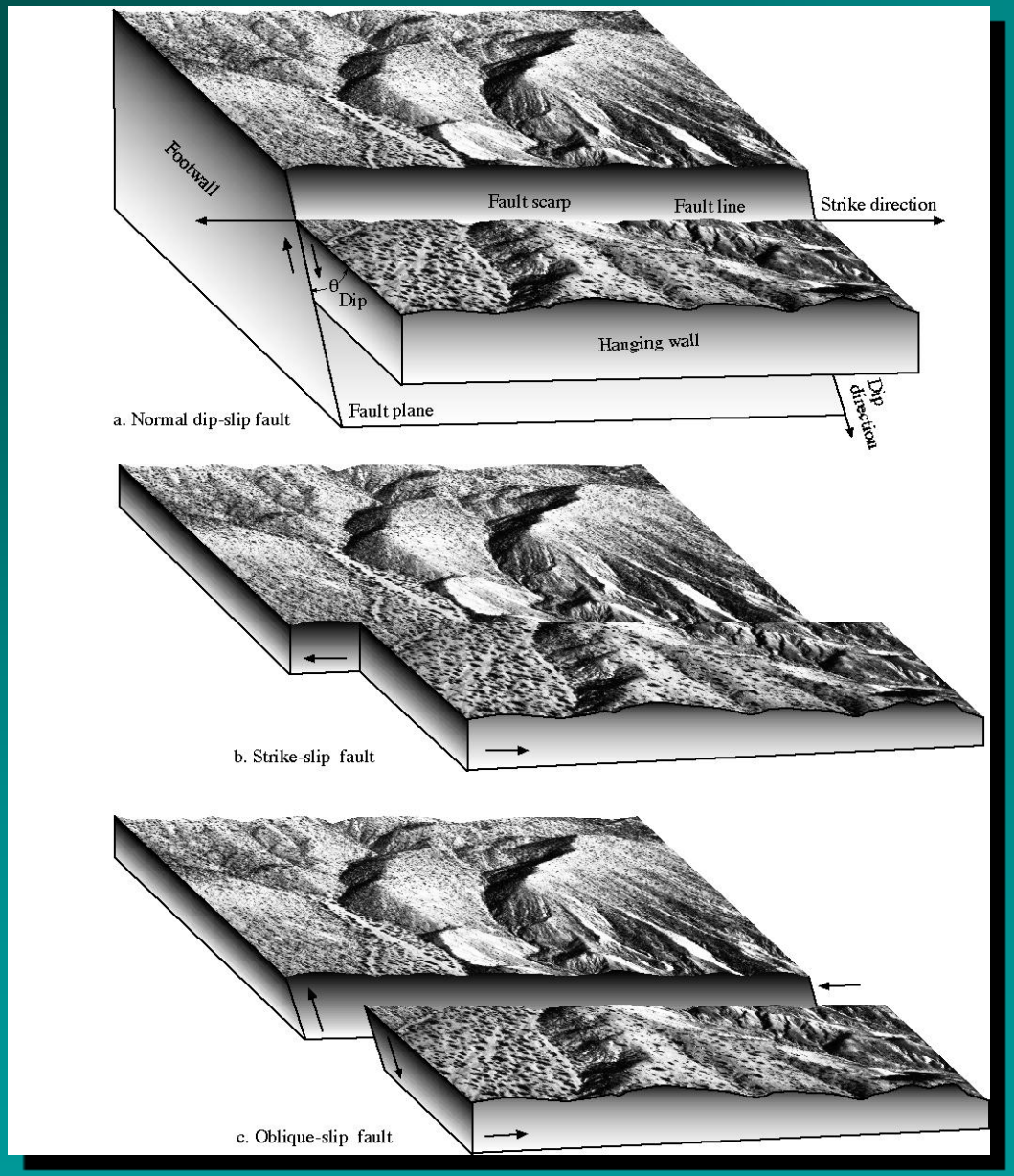

Jensen, 2000

Normal Fault Along the Wasatch Mountain Range in Utah as Recorded on Landsat Thematic Band 4 Imagery

Jensen, 2000

Landsat Thematic Mapper Image of the Intersection of the San Andreas and Garlock Faults

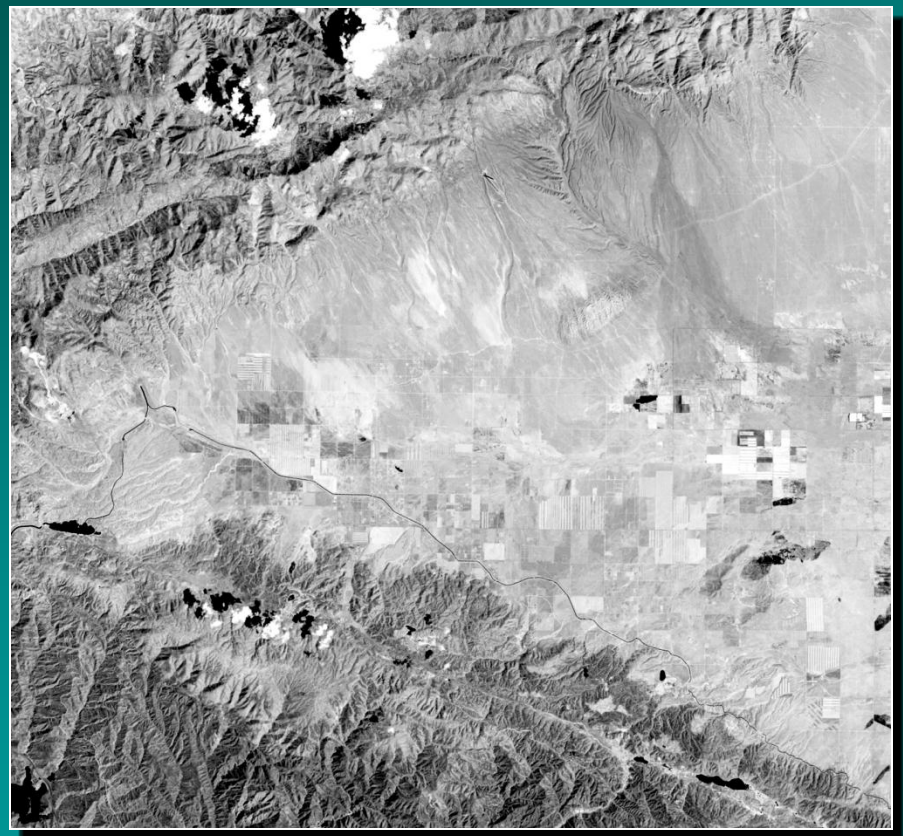

Landsat band 4 image

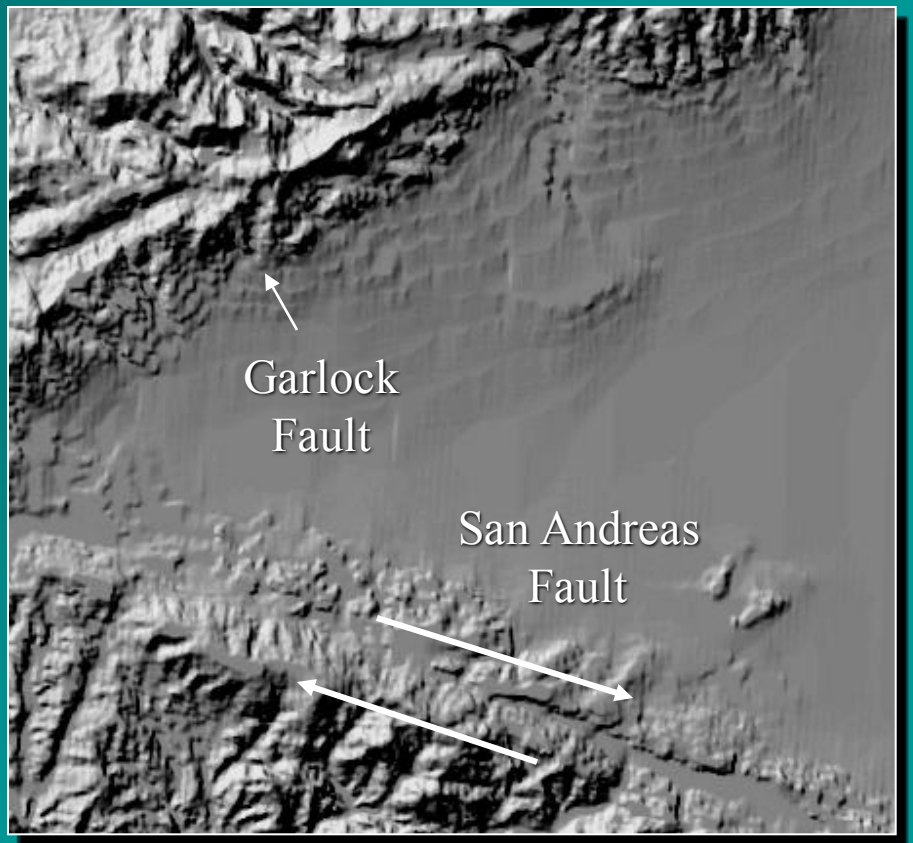

Shaded relief map derived from a digital elevation model

Remote Sensing of Igneous Landforms

Panchromatic Stereopair of the Devil's Tower,WY Intrusive Volcanic Neck Obtained on September 15, 1953 (south is at the top).

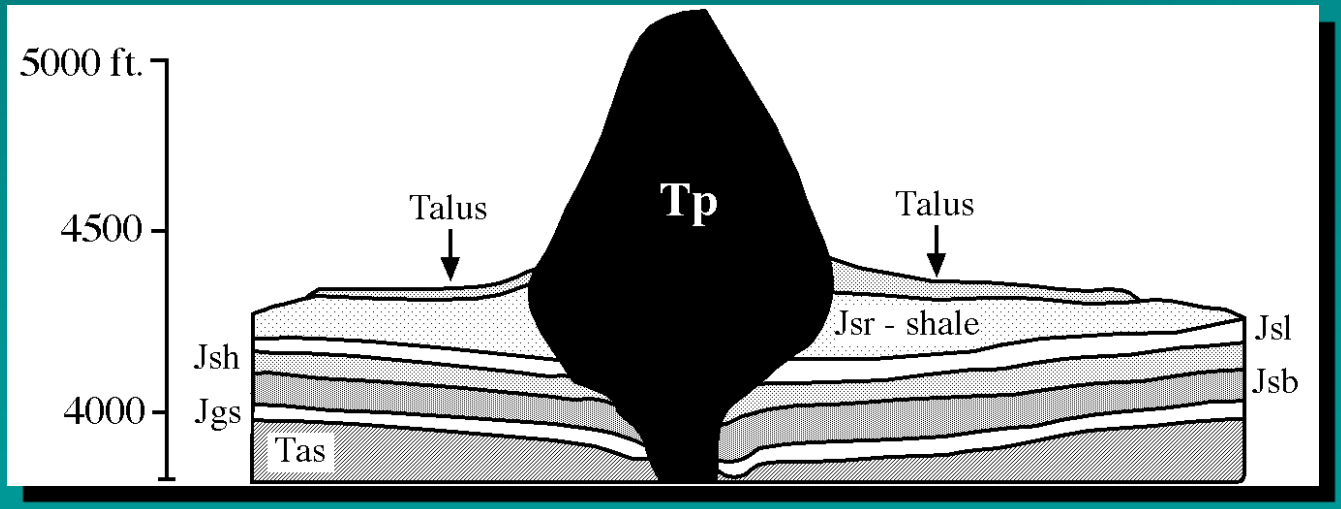

Jensen, 2000

Panchromatic Stereopair of the Menan Butte Tuff Cinder Cone Volcano in Idaho Obtained on June 24, 1960.

Composite Space Shuttle SIR-C/X-SAR image (bands C, X, L) of Kilauea Hawaii volcano on April 12, 1994

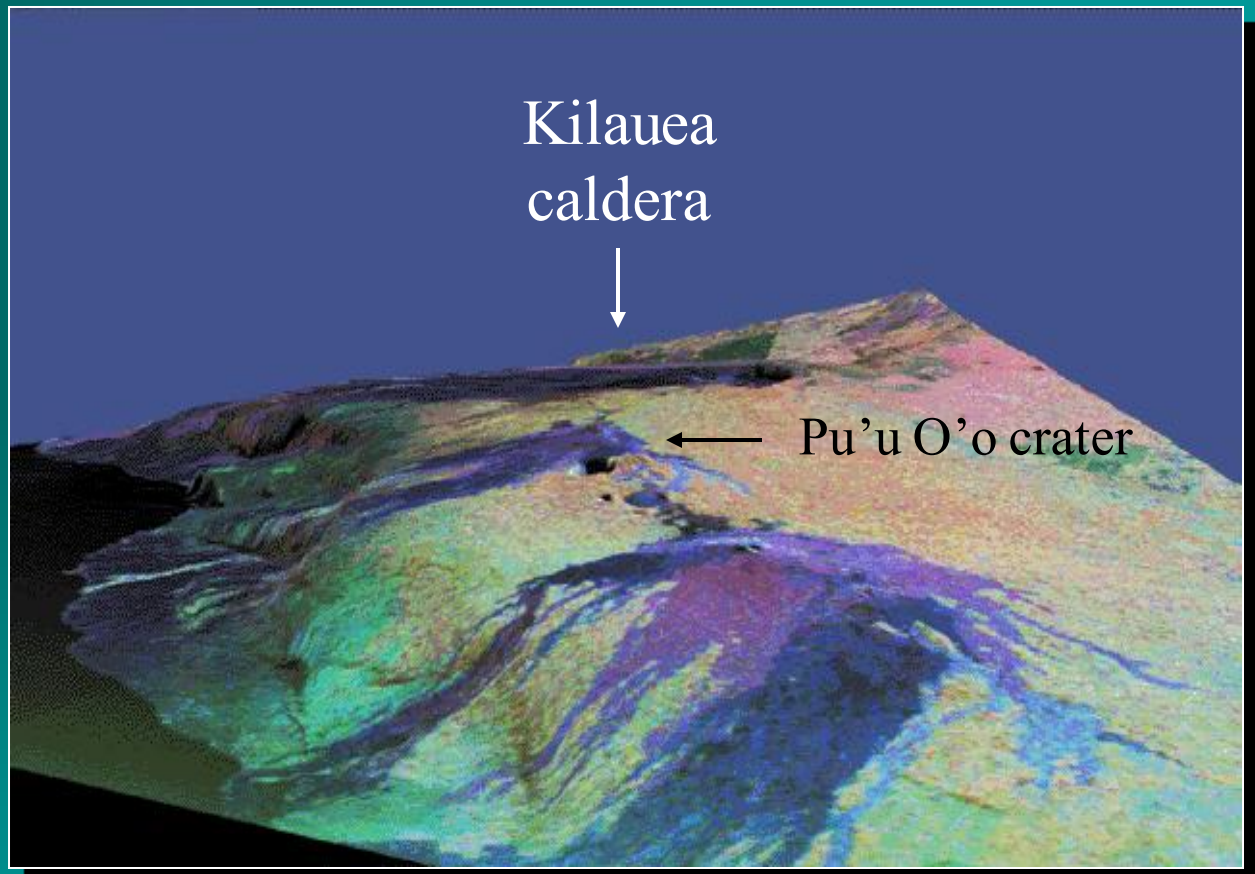

SIR-C image overlaid on a digital elevation model. Overland flow of lava on the shield volcano is evident.

Jensen, 2000

Jensen, 2000

Kilauea Pu'u O'o crater

Aerial photography of the overland flow of lava on the Kilauea Hawaii volcano

Three-dimensional Perspective View of Isla Isabela of the Galapagos Islands Obtained by the Space Shuttle SIR-C/X-SAR (draped over a digital elevation model)

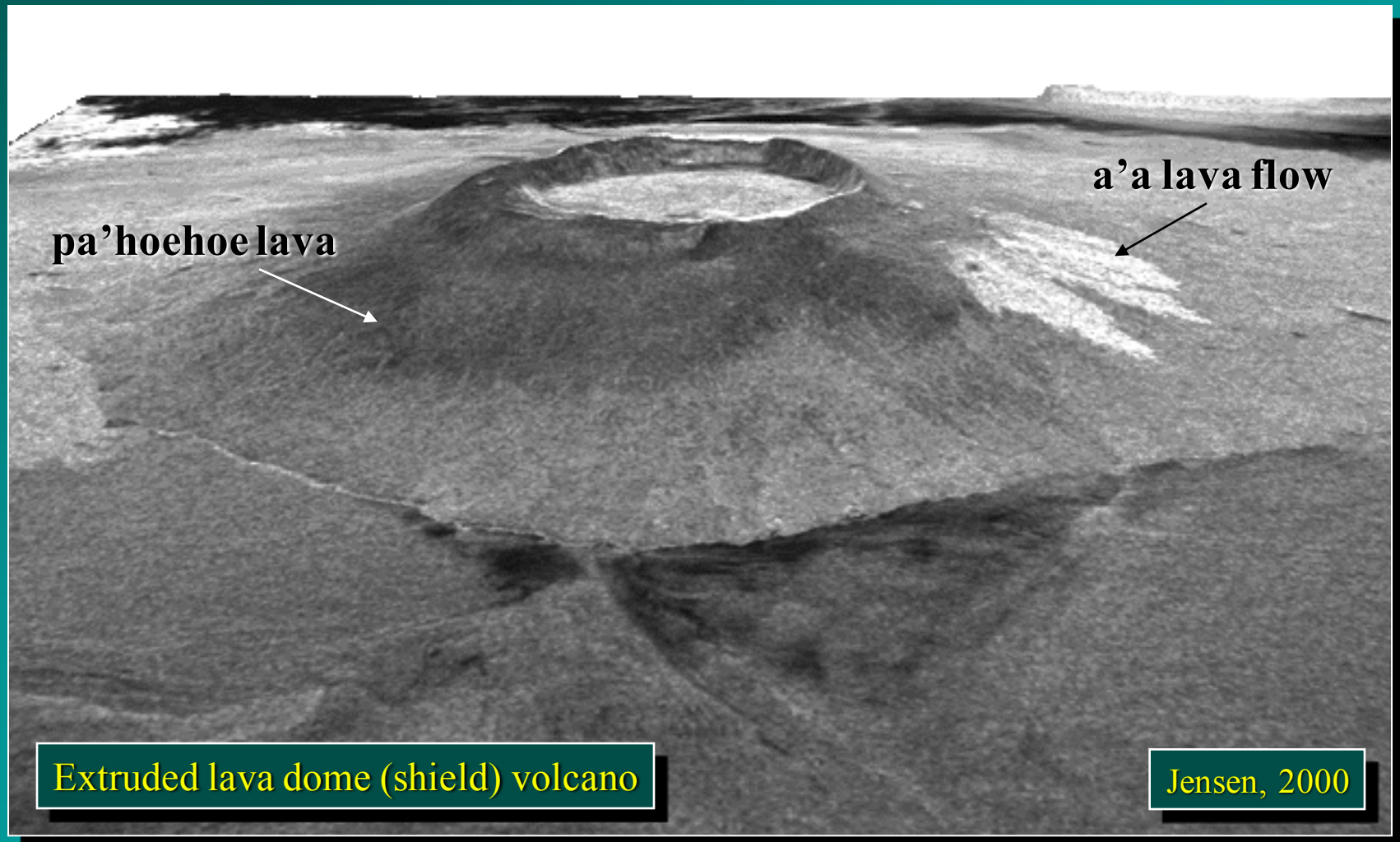

Jensen, 2000

Mount St. Helens erupting May 18, 1980 (U.S.G.S.)

USGS High Altitude Photography Stereopair of Composite Cone Mount St. Helens in Washington August 6, 1981

Remote Sensing of Landforms Developed on Horizontal Strata

Landsat Thematic Mapper Color Composites of a Portion of the Grand Canyon

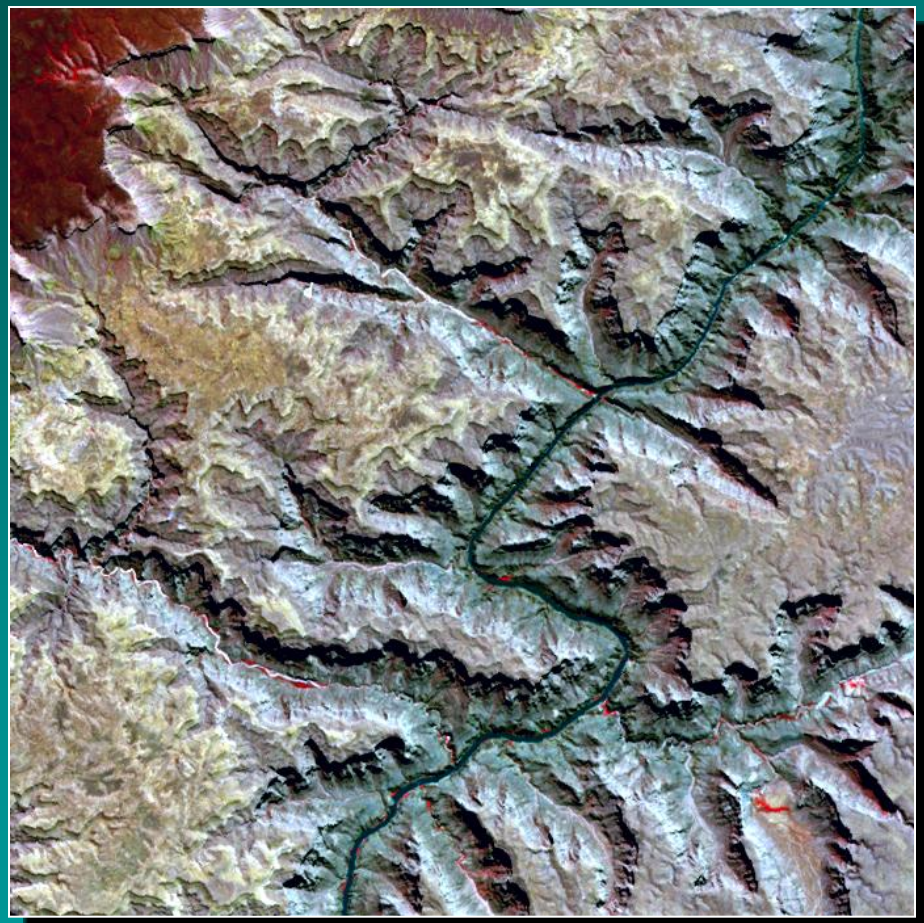

TM Bands 4,3,2 (RGB)

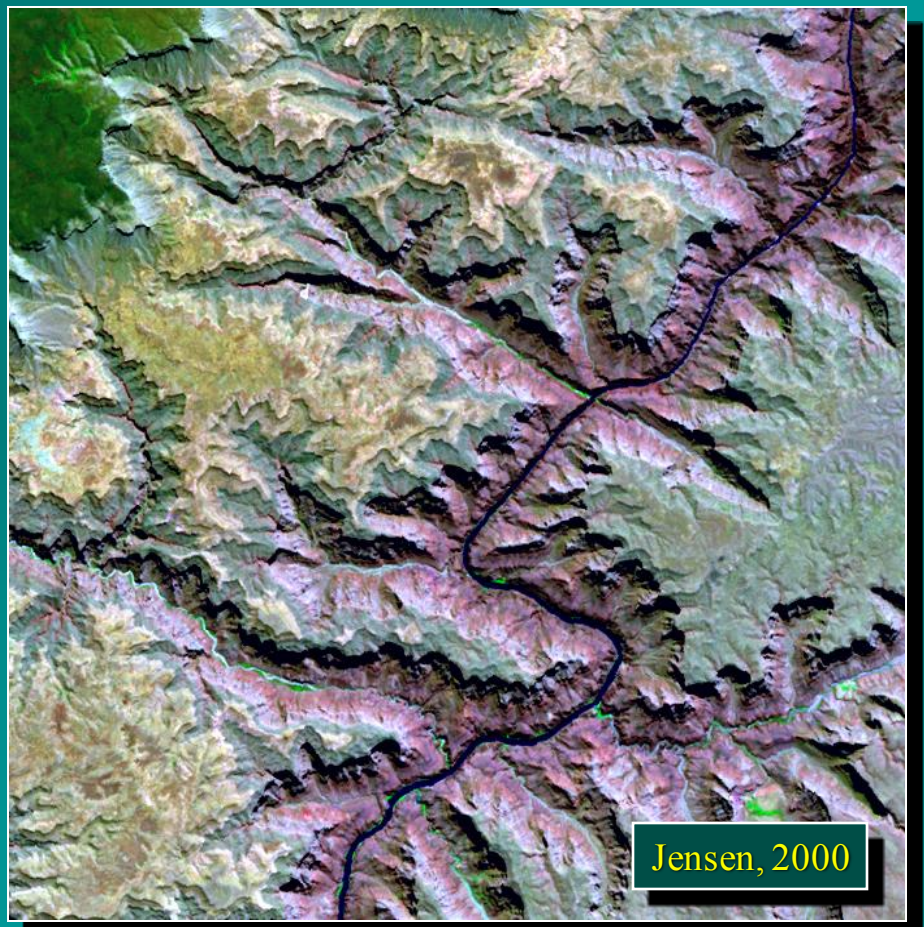

TM Bands 7,4,2 (RGB)

Geologic Cross-section of the Grand Canyon in Arizona

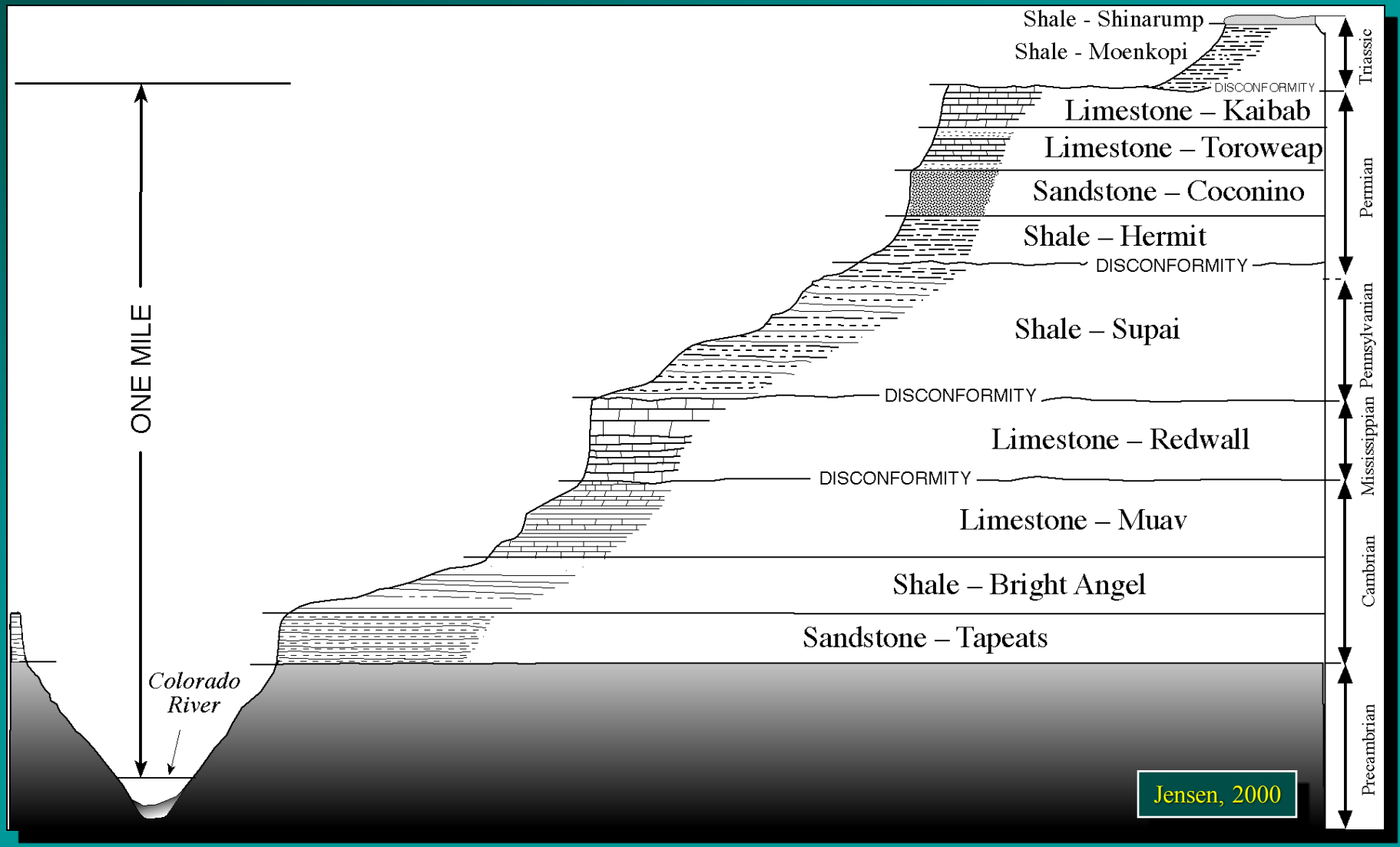

Panchromatic Stereopair of the Grand Canyon in Arizona

South Rim →

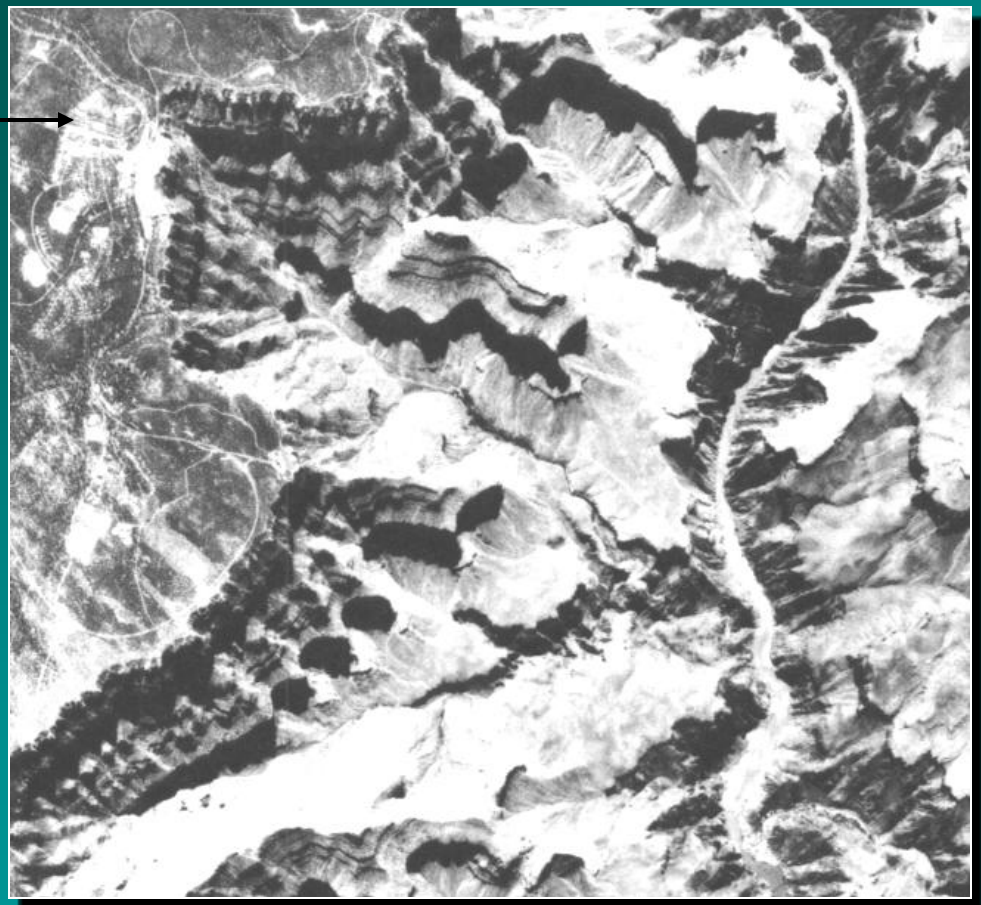

Jensen, 2000

Grand Canyon on the Colorado River in Arizona

Landsat TM Band 4

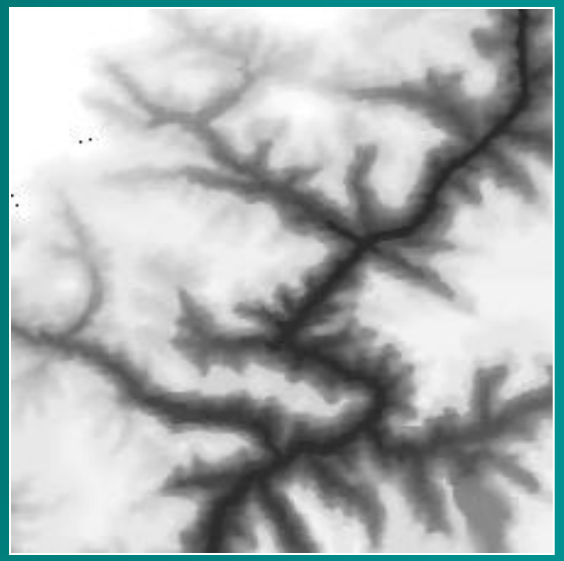

Digital Elevation Model

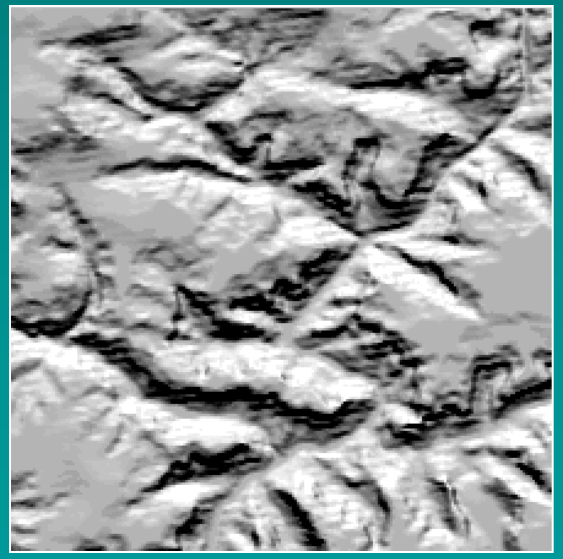

Shaded Relief Map

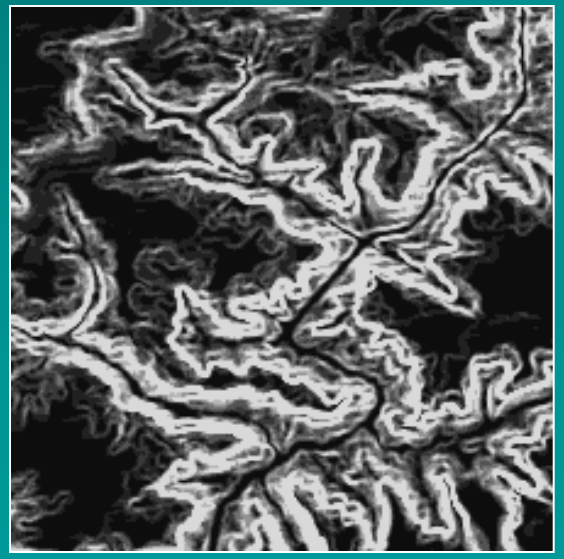

Slope Map

Jensen, 2000

Remote Sensing of Landforms Developed on Folded Strata

Panchromatic Stereopair of a Folded Landscape Near Maverick Spring, WY

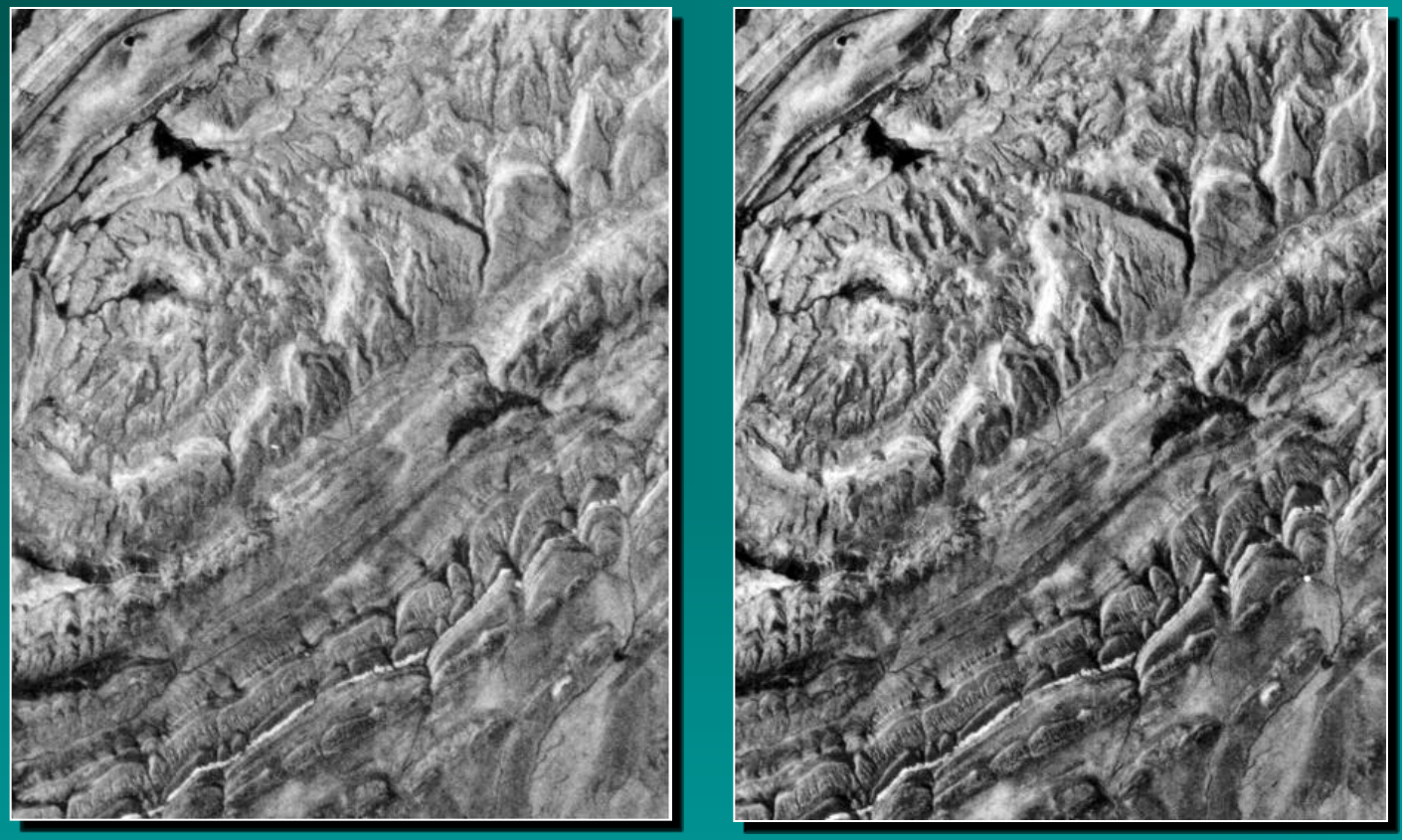

Jensen, 2000

This dissected asymmetric dome is an erosional remnant of a lunging anticline. Note the fine-textured topography, the strike of the ridges and valleys, the radial and trellis drainage controlled by the anticlinal structure, and the prominent hogback ridges.

Panchromatic Stereopair of a Synclinal Valley in the Appalachians near Tyrone, PA

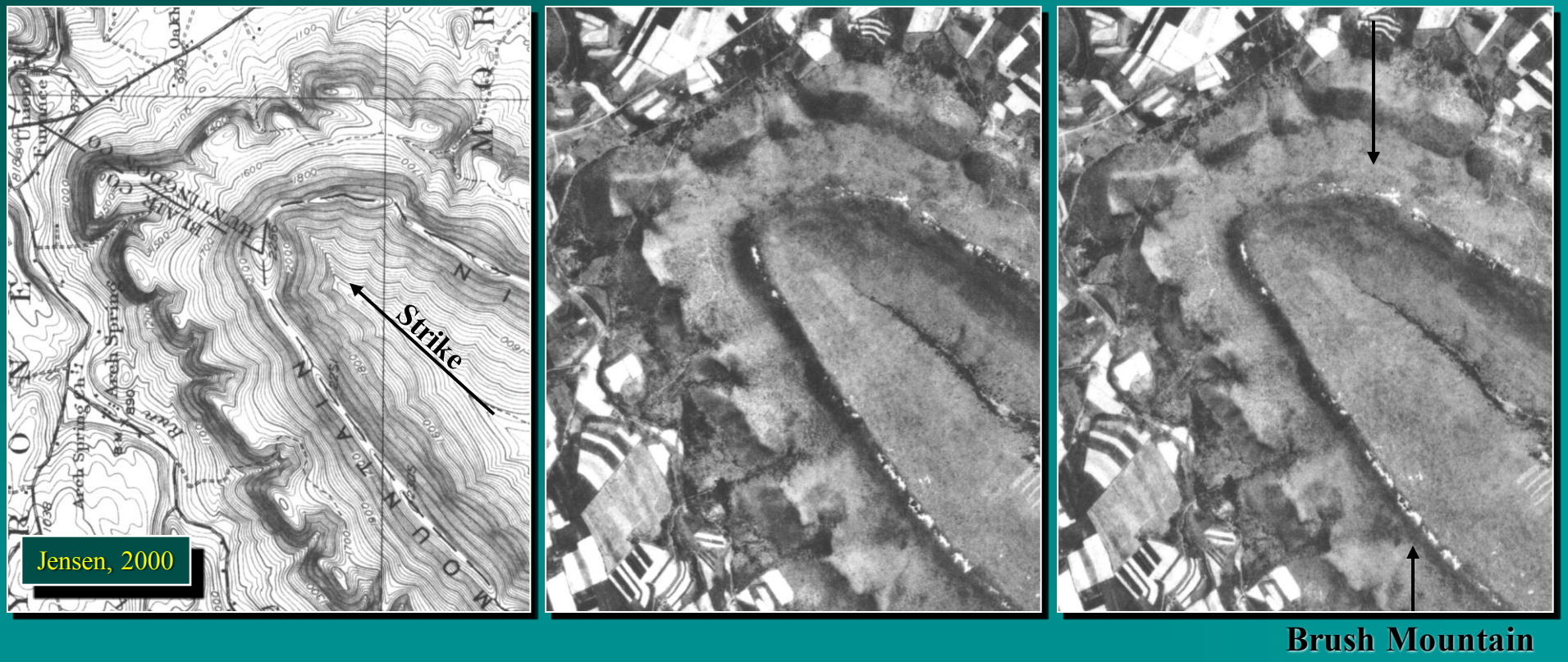

The ridge lines of Brush Mountain on the west and Canoe Mountain on the east are composed of more resistant sandstone while the less resistant, soluble limestone sedimentary rock has been eroded. The inter-bedding of the sandstone and limestone results in hogback ridges at the periphery of the syncline with a trellis drainage pattern.

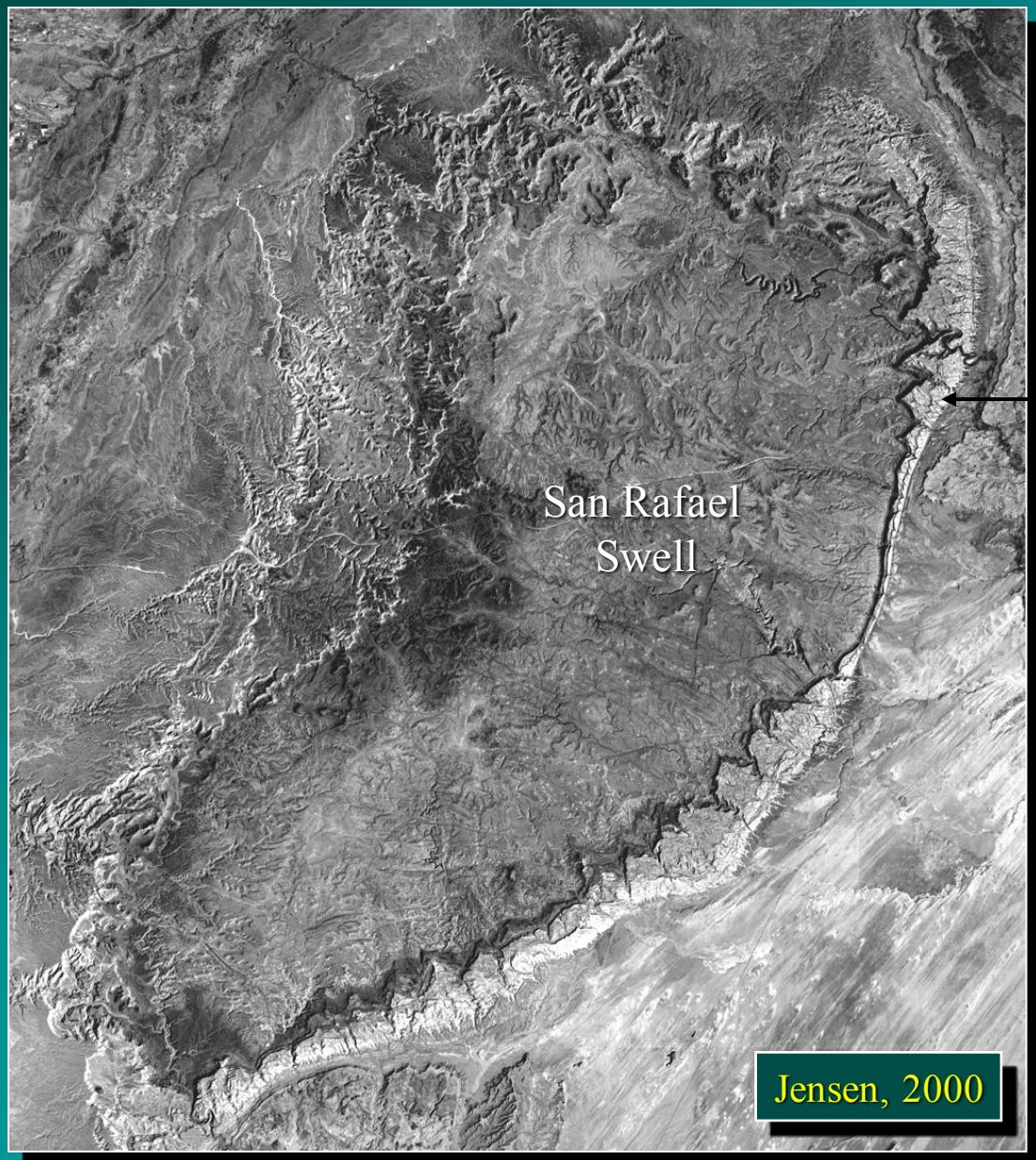

Landsat Thematic Mapper Band 4 Image of the San Rafael Swell in Southern Utah

Hogback ridges

The swell is a large flat-topped monoclinal upwarp bounded by hogback ridges on the southern and eastern flanks. The more resistant hogback ridges are composed of sandstone, while the less resistant shale beds have been eroded.

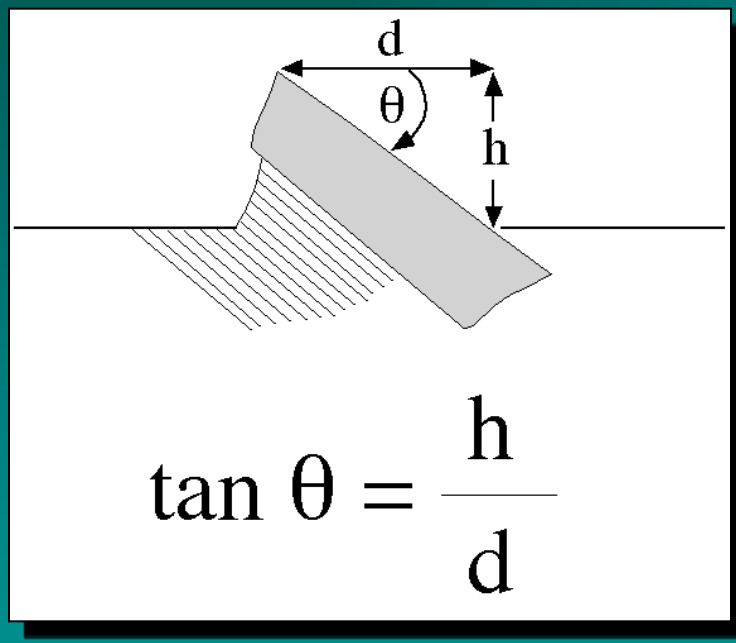

Jensen, 2000

The angle of dip, θ of a resistant bed such as a hogback may be calculated from stereoscopic imagery using photogrammetric measurement techniques where h is the vertical distance and d is the horizontal distance.

Remote Sensing of Fluvial Landforms

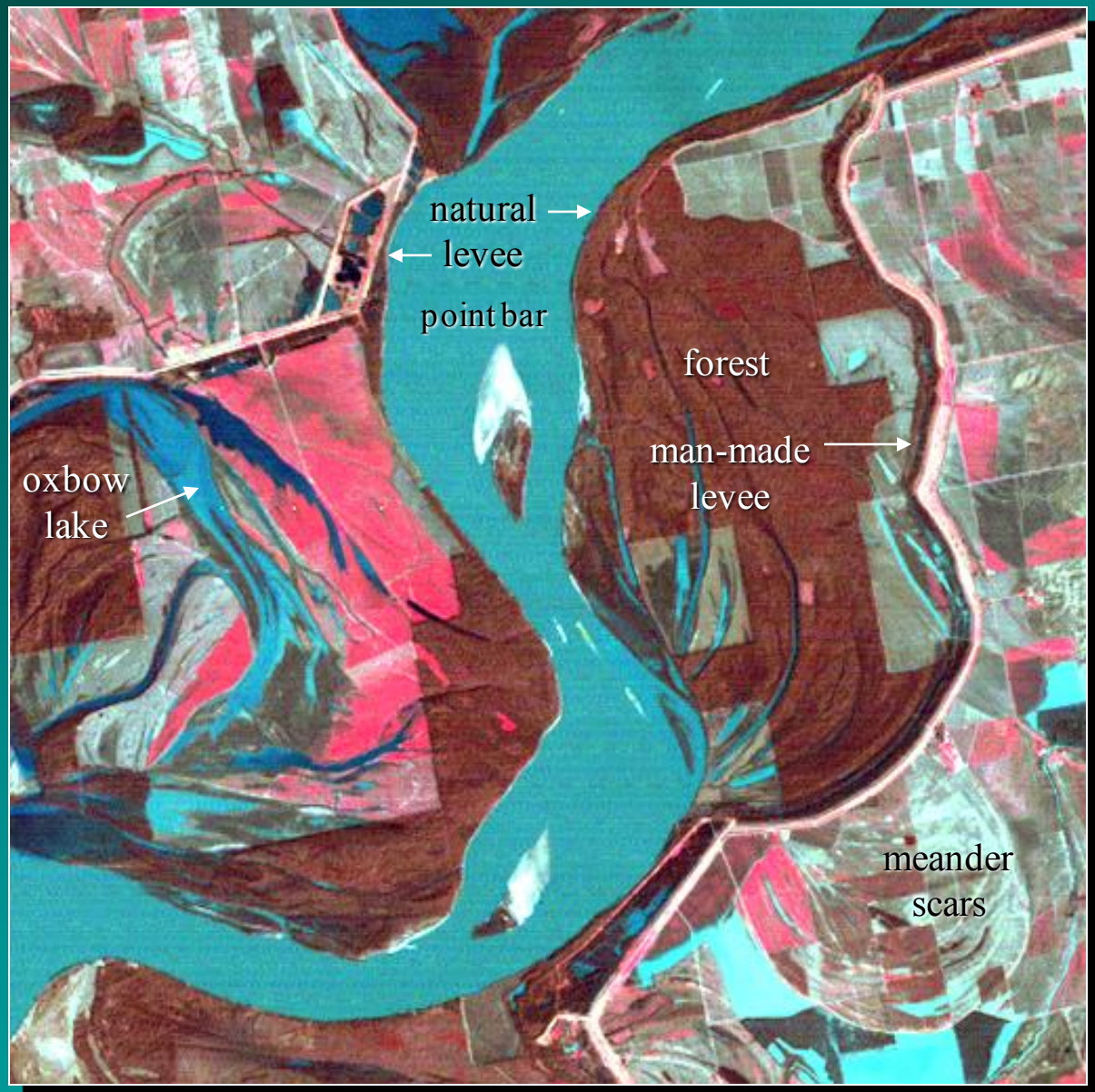

Landsat Thematic Mapper Imagery of the Mississippi River Bands 4,3,2 (RGB) January 13, 1983

Jensen, 2000

Deltas

Mississippi River Delta, U.S.

bird's foot delta

Niger River Delta, Africa

lobate delta

Nile River Delta, Egypt

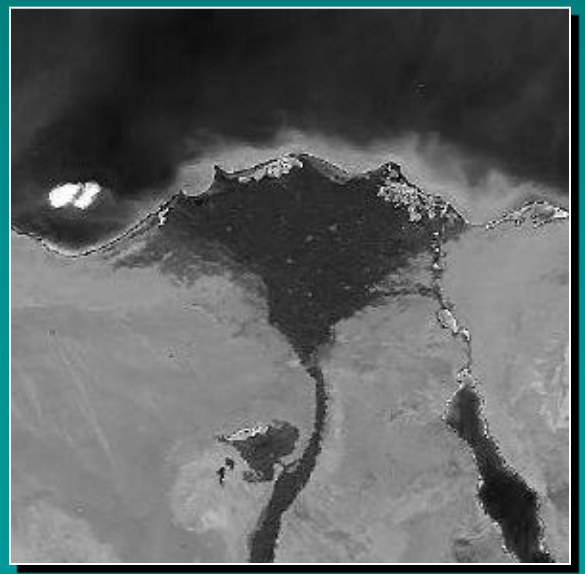

lobate delta

Irrawaddy River Delta, Burmah

crenulate delta

Jensen, 2000

Landsat Thematic Mapper Band 4 Imagery of Alluvial Fans, Pediments, and Playas

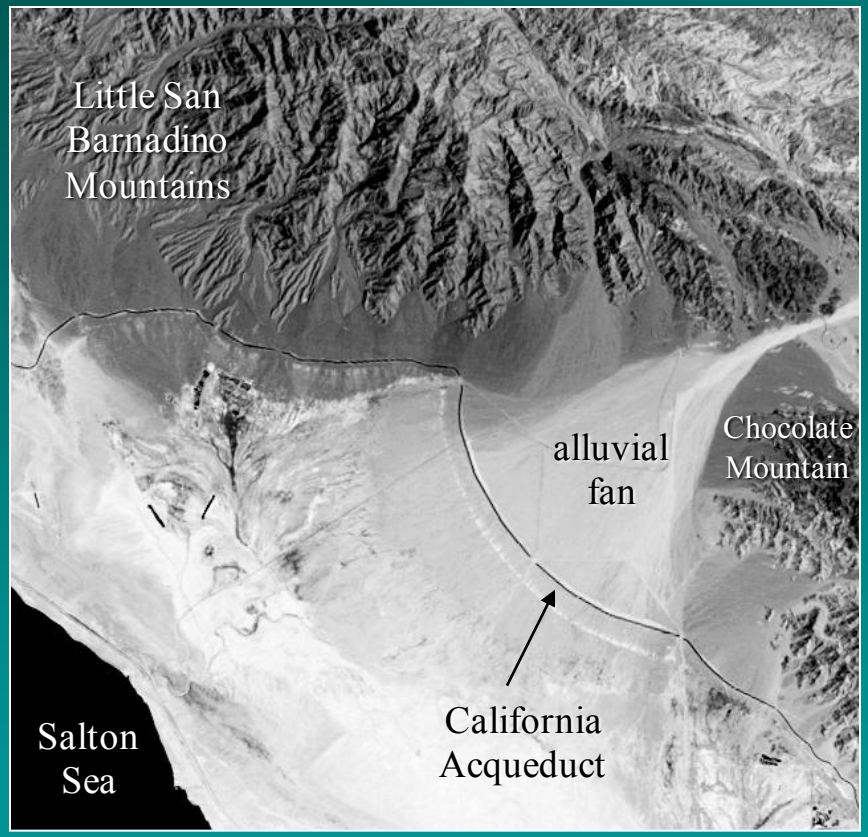

Alluvial fan between the Little San Bernadino and Chocolate Mountains northeast of the Salton Sea in California

Alluvial fan, several pediments, and a playa associated with an area in the White Mountain Range northwest of death Valley, California

Remote Sensing of Shoreline Landforms

Landsat Thematic Mapper
Color Composites of Morro Bay,California

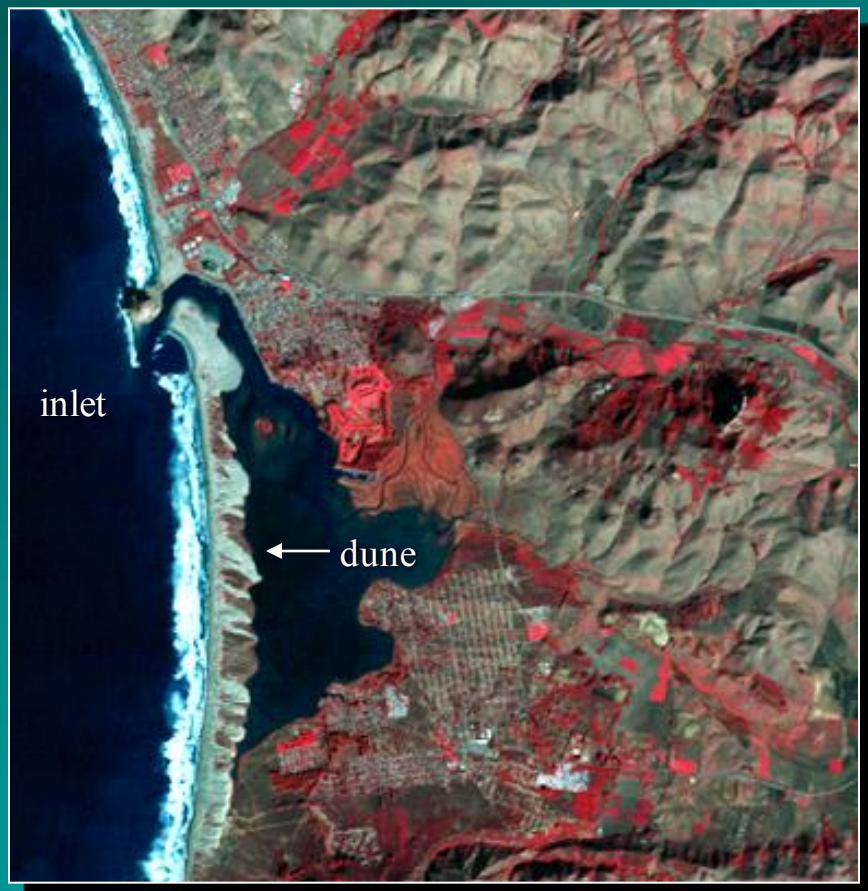

Bands 4,3,2 (RGB)

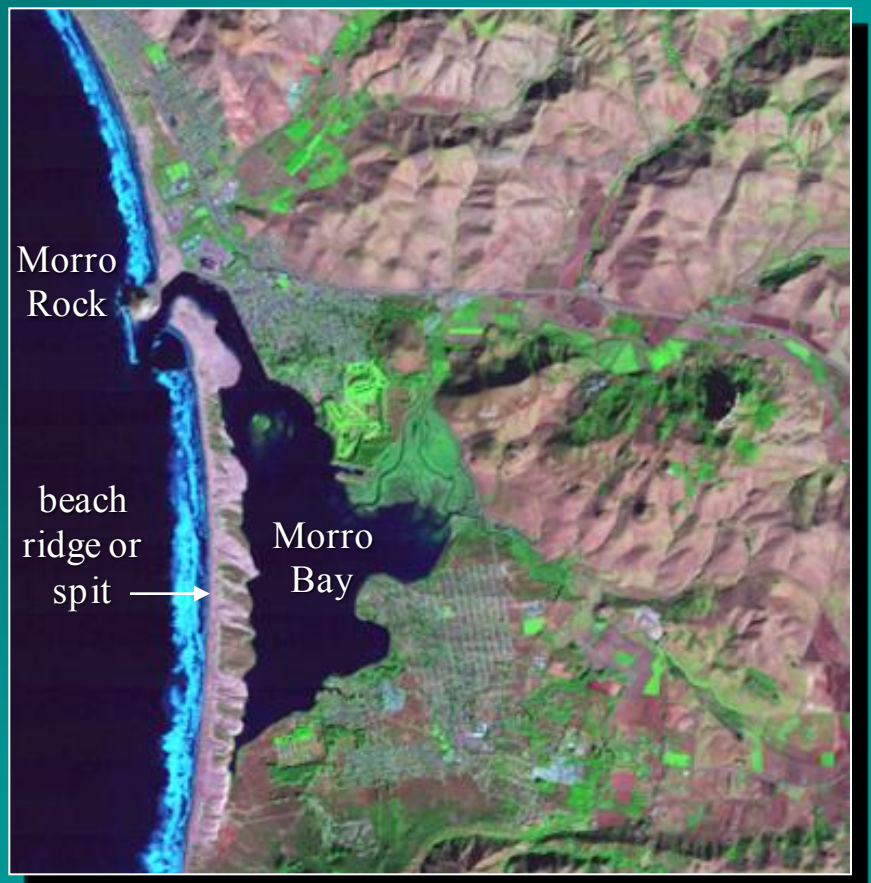

Bands 7,4,3 (RGB)

Jensen, 2000

NAPP Color-infrared Orthophotograph of Sullivan's Island, SC

Intercoastal Waterway

Isle of Palms

Jensen, 2000

NASA ATLAS Multispectral Scanner Data (3 x 3 m; Bands 6,4,2 = RGB) of the Tidal Flats Behind Isle of Palms, SC

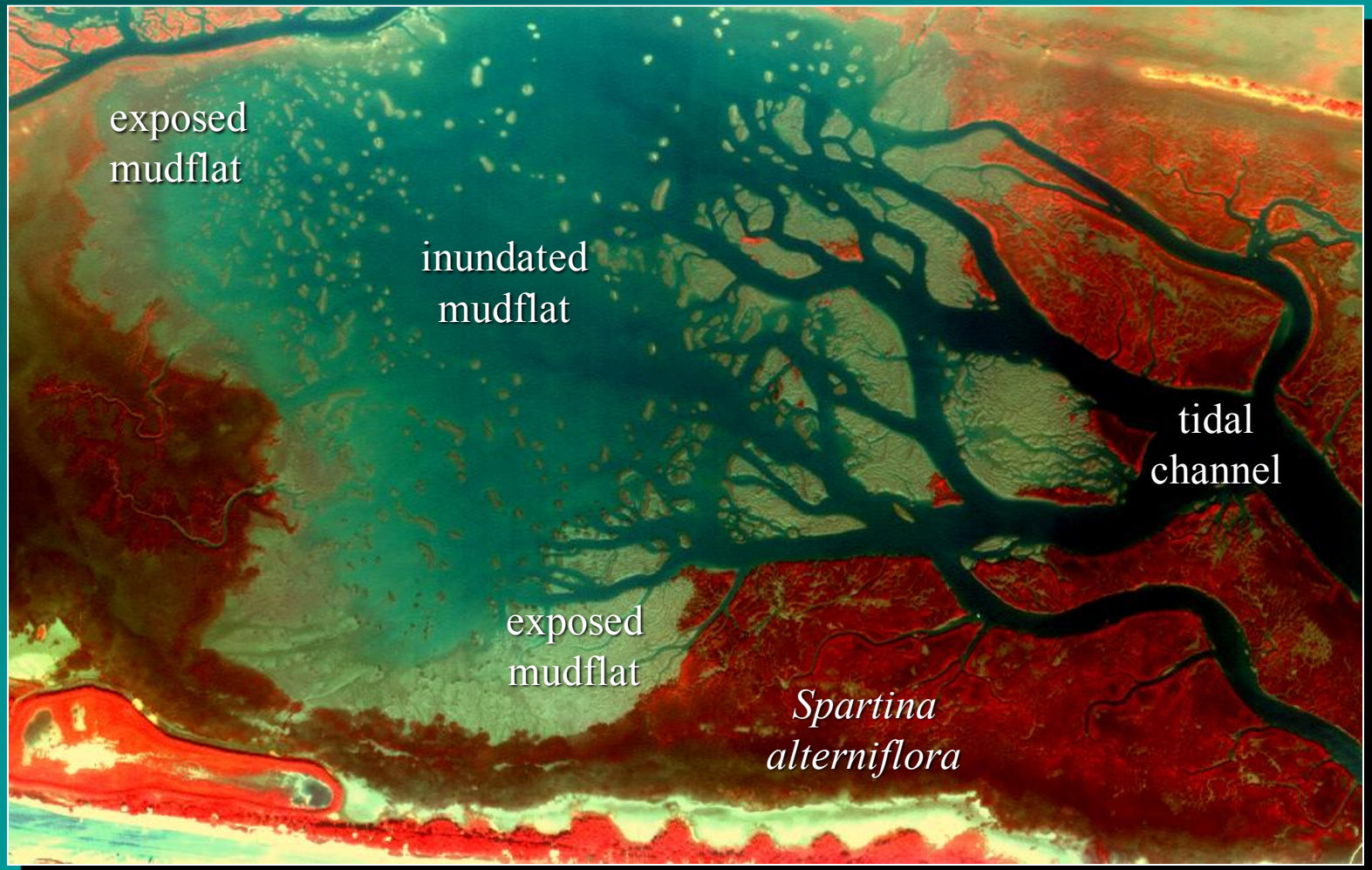

Jensen, 2000

Reefs and Atolls

Great Barrier Reef, Queensland, Australia

a.

Palancar Reef, Cozumel, Mexico

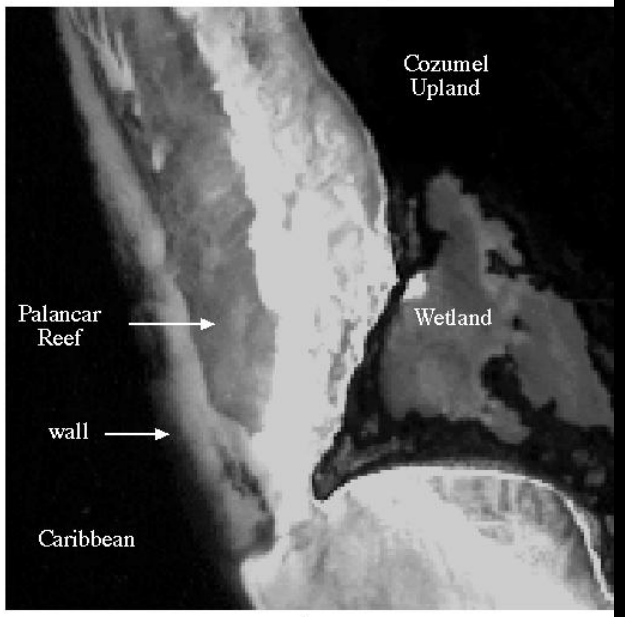

b.

French Mururoa Atoll in the South Pacific Ocean

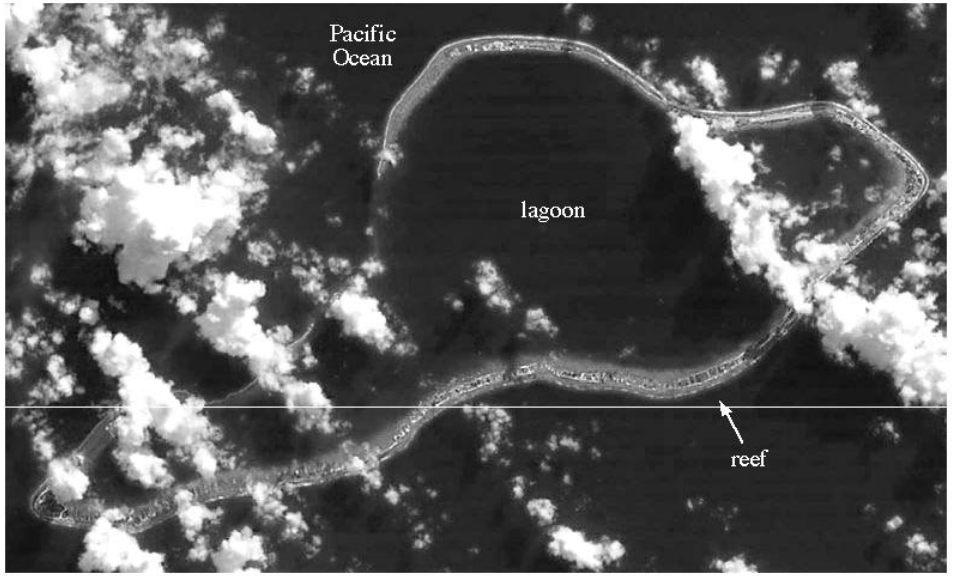

c.

Jensen, 2000

Remote Sensing of Glacial Landforms

Landsat MSS Image of the Uinta Mountain Range in Utah

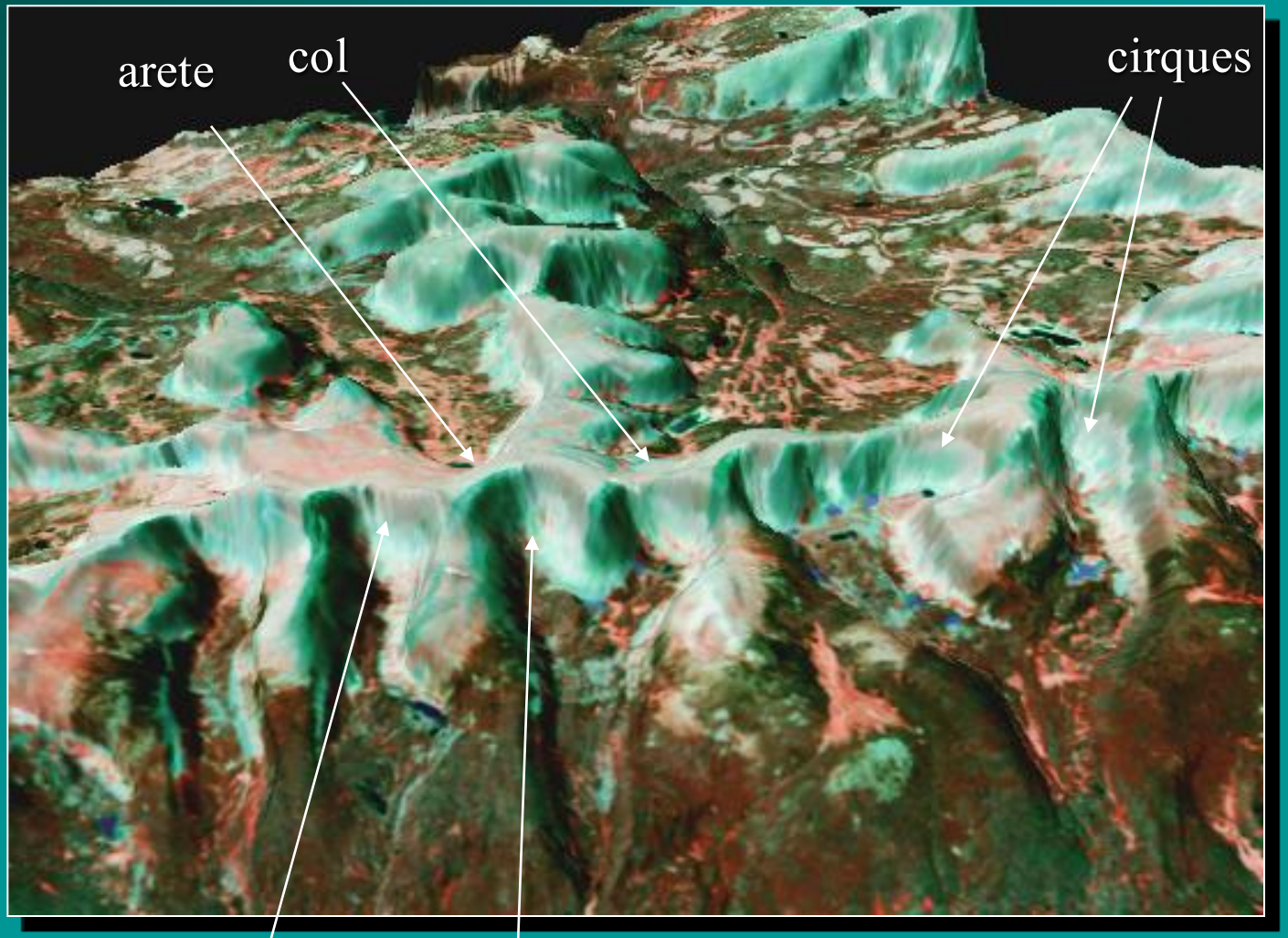

Jensen, 2000

Landsat Thematic Mapper Image of a Portion of the Wasatch Mountain Range in Utah

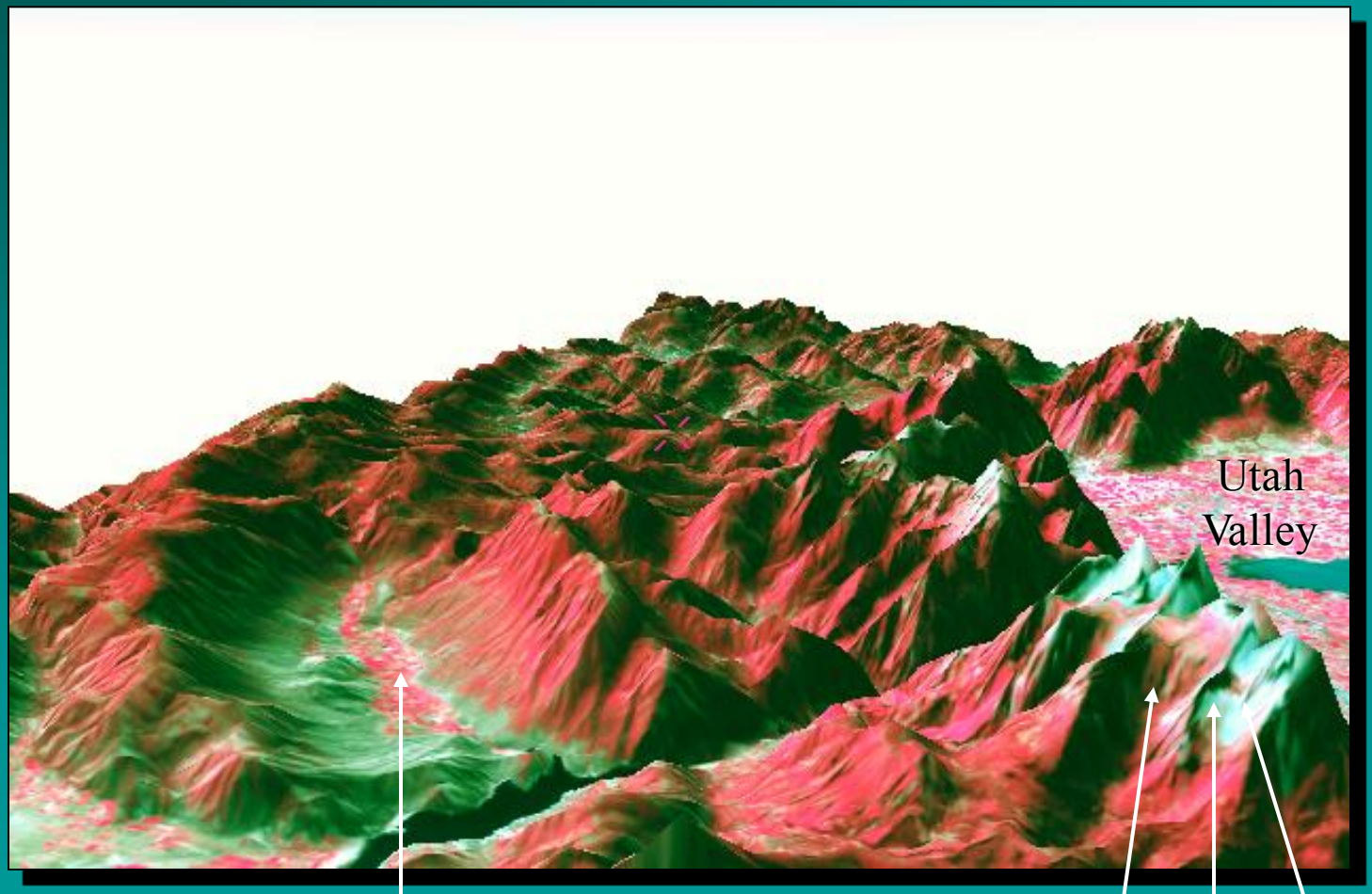

Jensen, 2000

Landsat MSS Image of Lake Tahoe in the Sierra Nevada of California

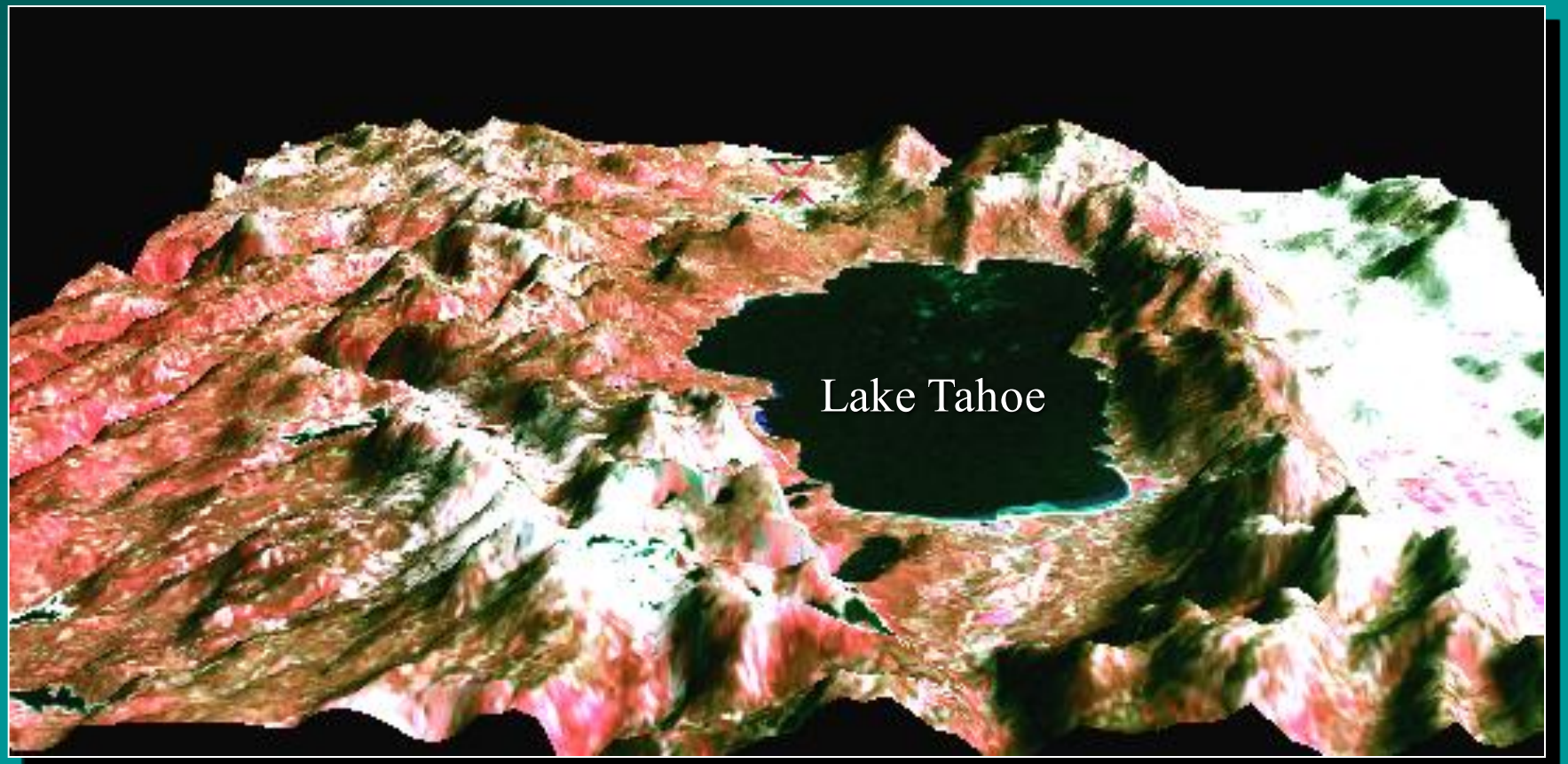

Jensen, 2000

Oblique Panchromatic Aerial Photography of Glacial Moraines

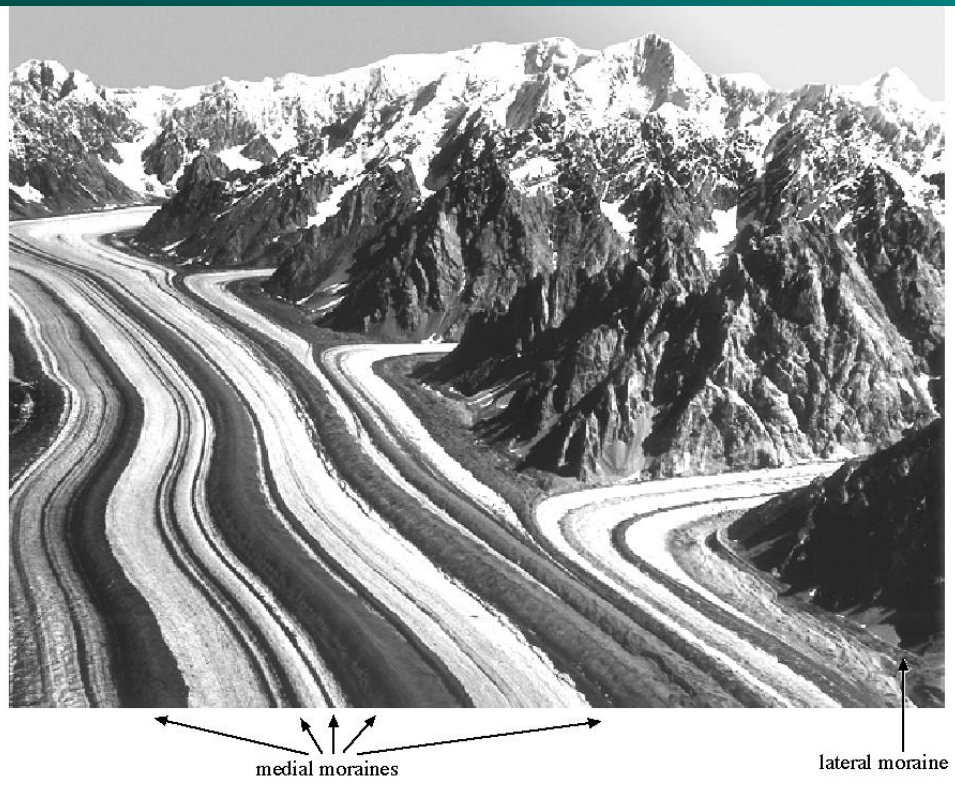

a. Lateral and medial moraines on Barnard Glacier, AK

b. Lateral and terminal glacial moraines on Bylot Island, Baffin Island, NW Territories, Canada.

Jensen, 2000

Oblique Panchromatic Aerial Photography of Glacial Eskers, Kettles, and Drumlins

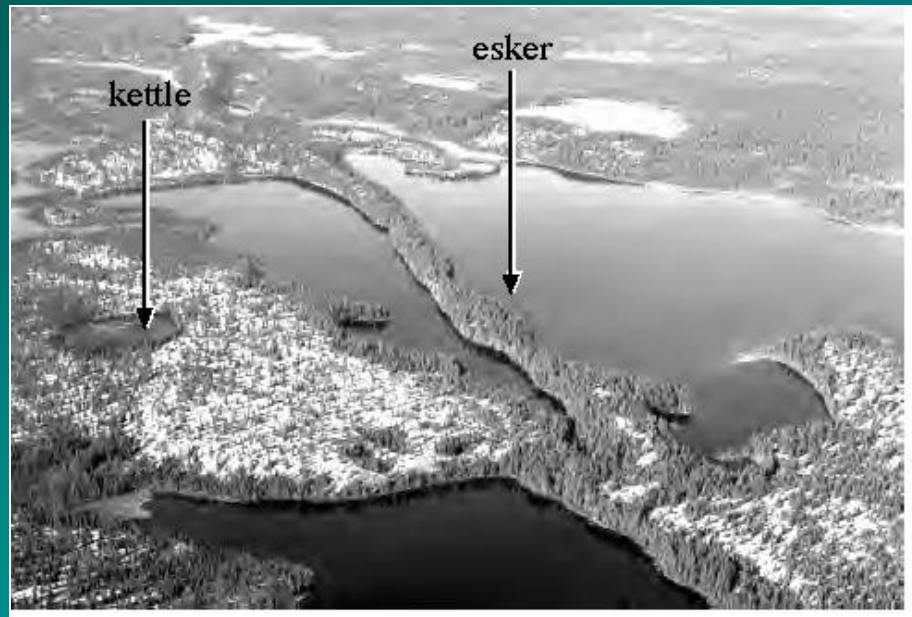

a. An esker and kettle in Northern Manitoba, Canada.

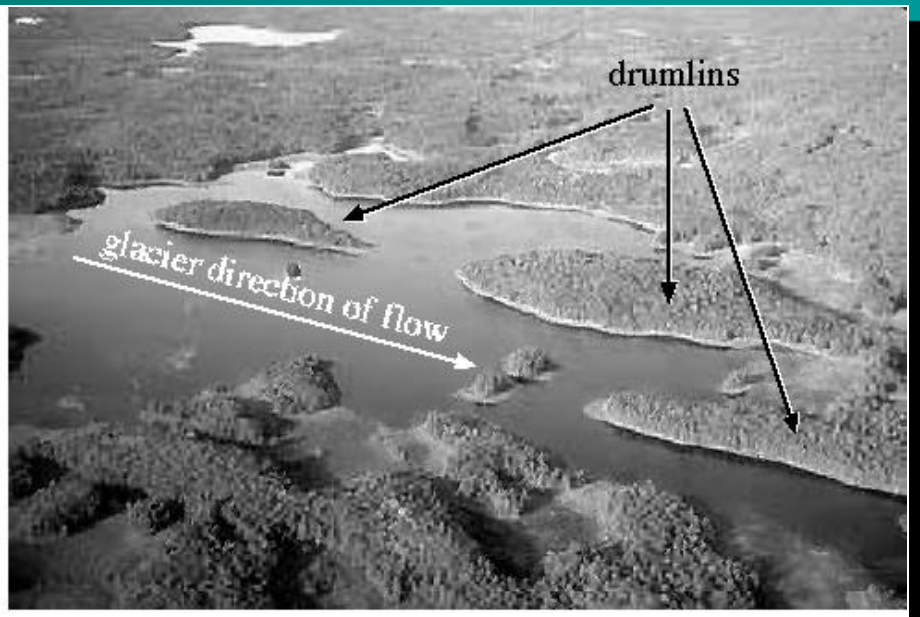

b. Drumlins in Kejimkujik National Park, Canada.

Jensen, 2000

Remote Sensing of Eolian Landforms

Crescentric Dunes

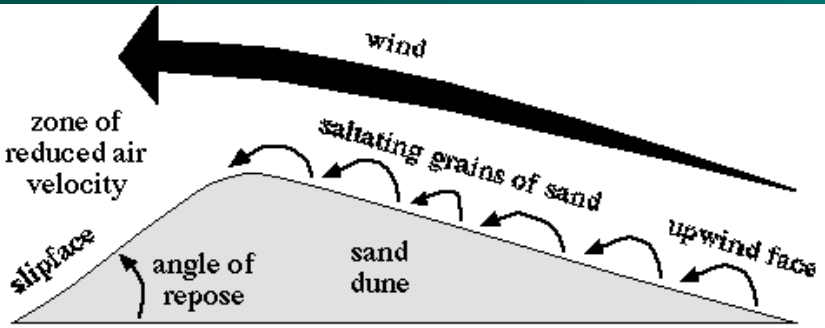

a. Sand movement on a dune.

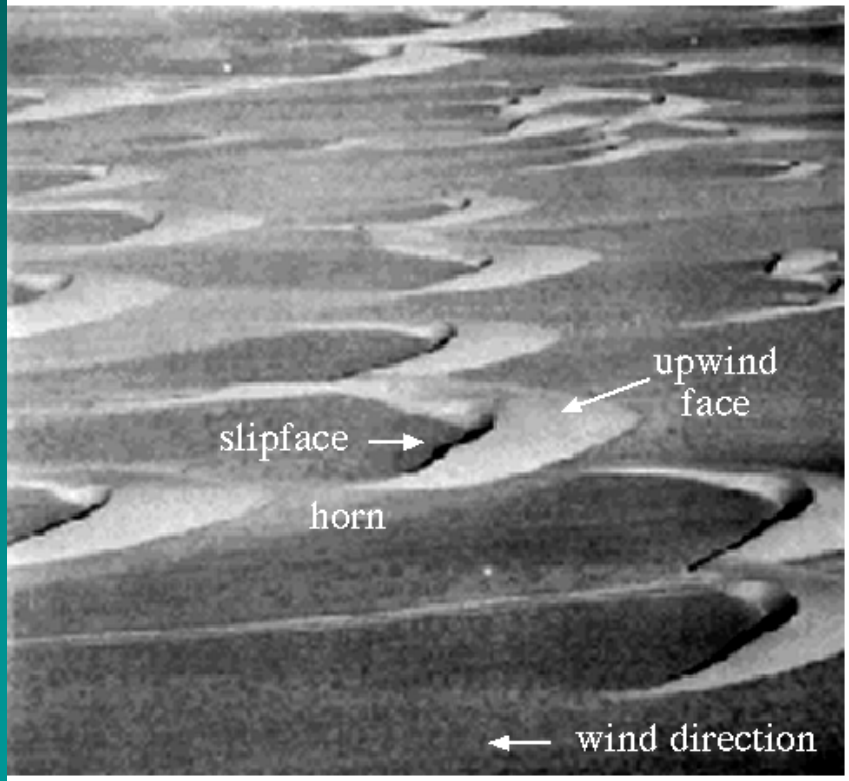

b. Oblique view of crescentric dunes (also called barchan or transverse dunes).

c. View of a single crescentric dune.

Jensen, 2000

Star Dunes

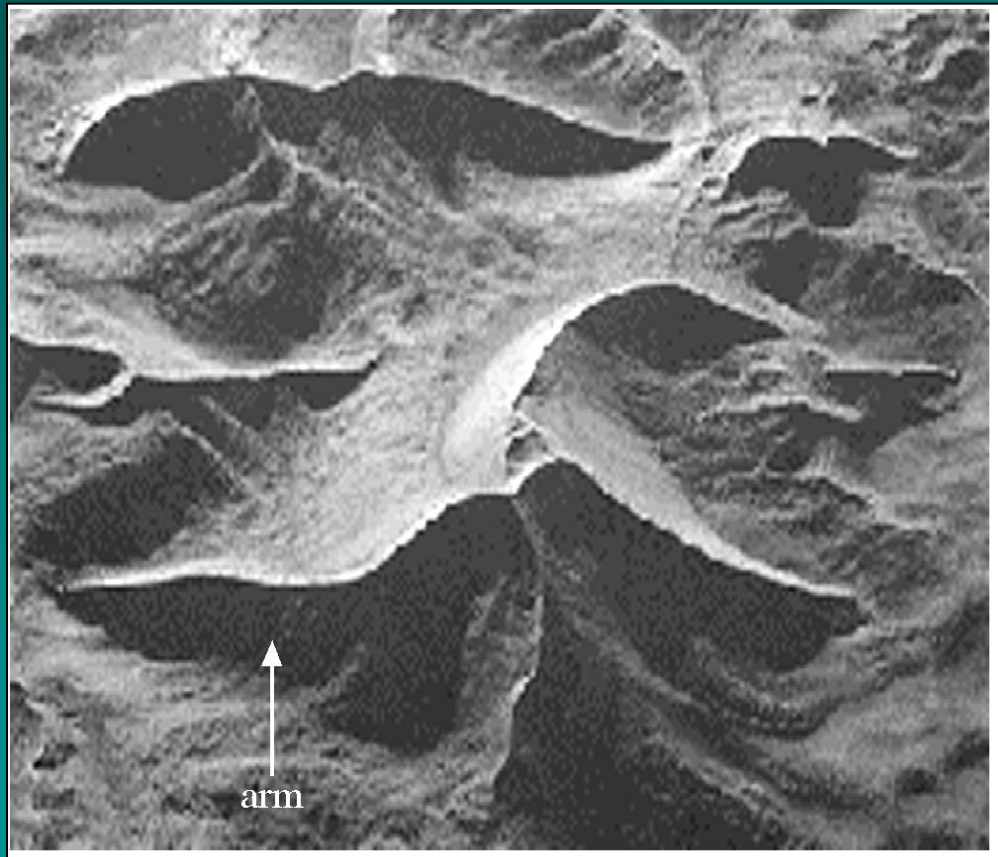

a. Star dunes in the Namib Desert.

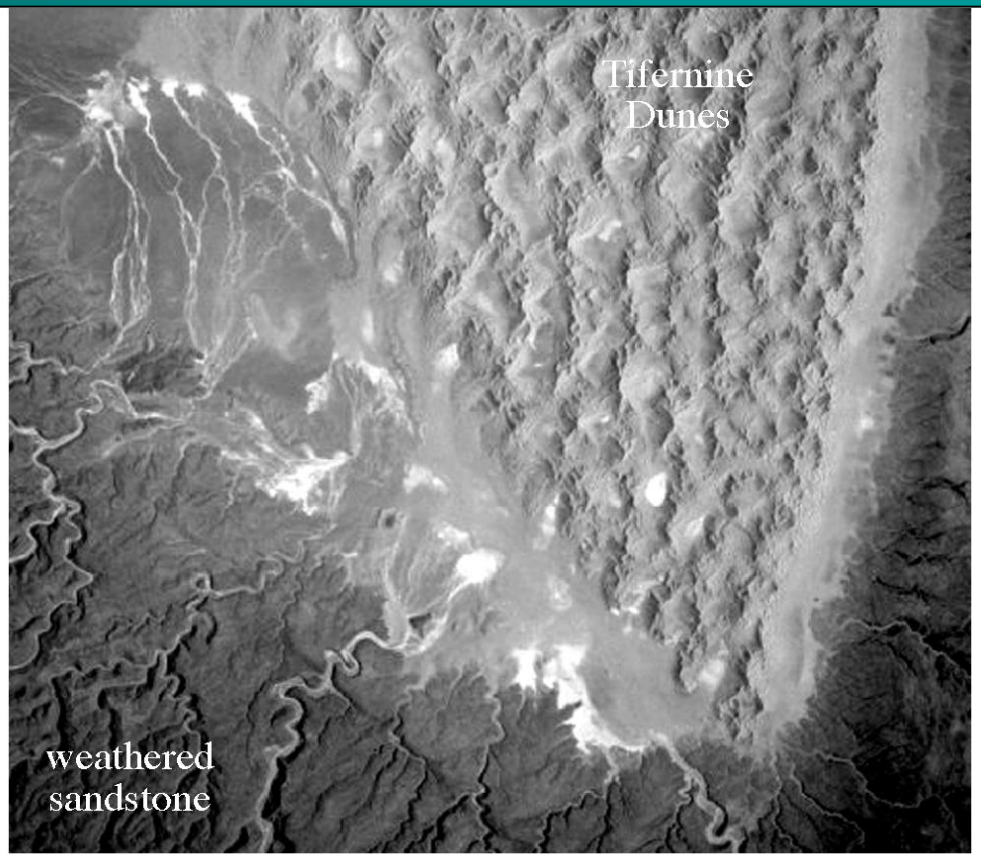

b. Space Shuttle photograph of the complex linear Tifernine Dunes in the Tassili N' Ajjer of southeastern Algeria superimposed with star dunes.

Linear (Longitudinal) and Dome Dunes

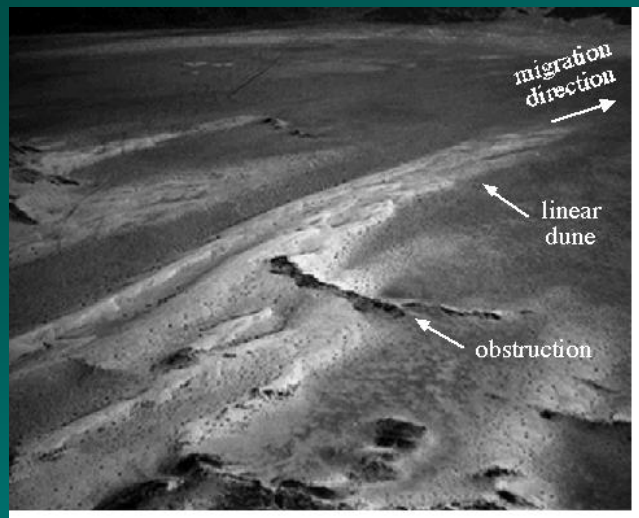

a. Oblique view of a linear (longitudinal) dune on Soda Lake.

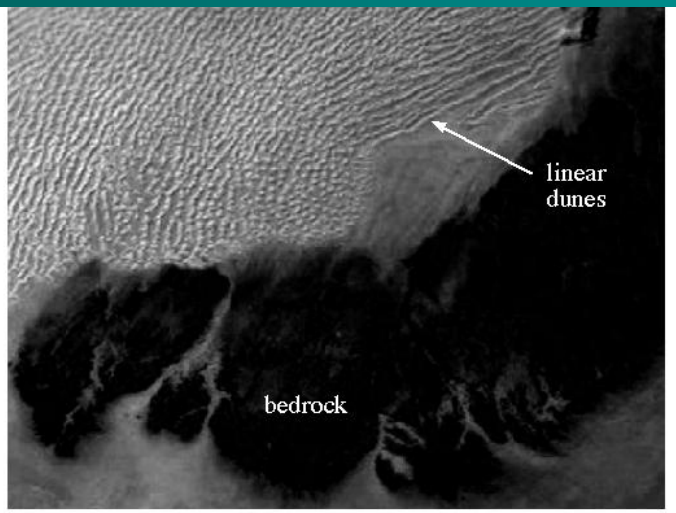

b. Space Shuttle photograph of linear dunes in the Marzuq Desert, Libya.

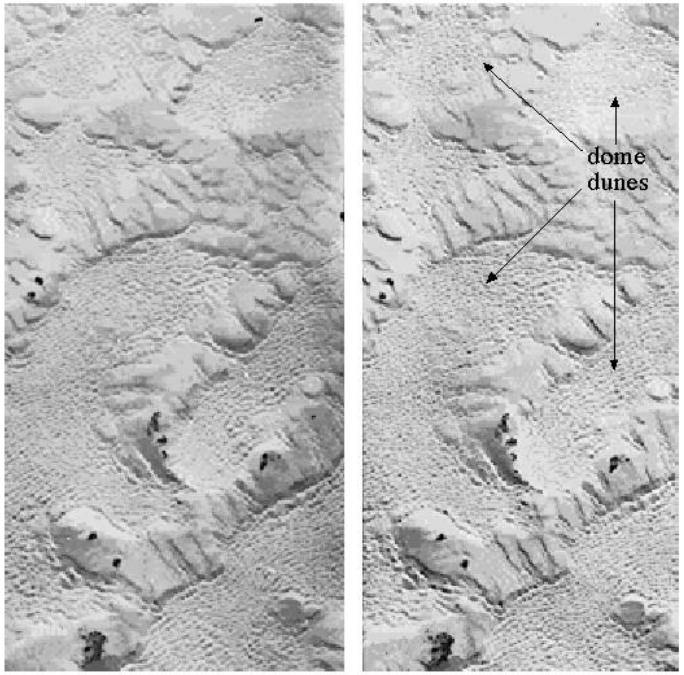

c. Stereopair of dome dunes in the Western Shield of Saudi Arabia (Army Map Service Photos).

Jensen, 2000